

H_∞ based control of a DC/DC buck converter feeding a constant power load in uncertain DC microgrid system

BOUKERDJA, Mahdi, CHOUDER, Aissa, HASSAINE, Linda, BOUAMAMA, Belkacem Ould, ISSA, Walid <<http://orcid.org/0000-0001-9450-5197>> and LOUASSAA, Khalil

Available from Sheffield Hallam University Research Archive (SHURA) at:

<http://shura.shu.ac.uk/26483/>

This document is the author deposited version. You are advised to consult the publisher's version if you wish to cite from it.

Published version

BOUKERDJA, Mahdi, CHOUDER, Aissa, HASSAINE, Linda, BOUAMAMA, Belkacem Ould, ISSA, Walid and LOUASSAA, Khalil (2020). H_∞ based control of a DC/DC buck converter feeding a constant power load in uncertain DC microgrid system. ISA Transactions.

Copyright and re-use policy

See <http://shura.shu.ac.uk/information.html>

Journal Pre-proof

H_{∞} based control of a DC/DC buck converter feeding a constant power load in uncertain DC microgrid system

Mahdi Boukerdja, Aissa Chouder, Linda Hasseine,
Belkacem OuldBouamama, Walid Issa, Khalil Louassaa



PII: S0019-0578(20)30215-9
DOI: <https://doi.org/10.1016/j.isatra.2020.05.031>
Reference: ISATRA 3592

To appear in: *ISA Transactions*

Received date : 4 July 2019
Revised date : 21 May 2020
Accepted date : 21 May 2020

Please cite this article as: M. Boukerdja, A. Chouder, L. Hasseine et al., H_{∞} based control of a DC/DC buck converter feeding a constant power load in uncertain DC microgrid system. *ISA Transactions* (2020), doi: <https://doi.org/10.1016/j.isatra.2020.05.031>.

This is a PDF file of an article that has undergone enhancements after acceptance, such as the addition of a cover page and metadata, and formatting for readability, but it is not yet the definitive version of record. This version will undergo additional copyediting, typesetting and review before it is published in its final form, but we are providing this version to give early visibility of the article. Please note that, during the production process, errors may be discovered which could affect the content, and all legal disclaimers that apply to the journal pertain.

© 2020 Published by Elsevier Ltd on behalf of ISA.

H_{∞} Based Control Of DC/DC Buck Converter Feeding A Constant Power Load In Uncertain DC Microgrid System.

Mahdi Boukerdja^{1,*}, Aissa Chouder¹, Linda Hassaine², Belkacem OuldBouamama³, Walid Issa⁴, Khalil Louassaa¹

¹ University of Msila-Algeria, Electrical Engineering Laboratory (LGE), BP166, 28000, Algeria.

² Centre de Développement des Energies Renouvelables, CDER. B.P. 62, Route de l'Observatoire, 16340 Bouzaréah, Algiers, Algeria.

³ Univ. Lille, CNRS, Centrale Lille, UMR 9189-CRISAL—Centre de Recherche en Informatique Signal et Automatique de Lille, F-59000 Lille, France

⁴ Electrical and Electronic Engineering Departement, Sheffield Hallam University, S11WB, UK.

mahdi.boukerdja@univ-msila.dz, aissa.chouder@univ-msila.dz,
l.hassaine@cder.dz, belkacem.ouldbouamama@polytech-lille.fr,
walid.issa@shu.ac.uk, khalil.louassaa@univ-msila.dz,

H_{∞} Based Control Of A DC/DC Buck Converter Feeding A Constant Power Load In Uncertain DC Microgrid System.

Abstract:

DC microgrids are gaining more and more popularity and are becoming a more viable alternative to AC microgrids (MGs) due to their advantages in terms of simpler power converter stages, flexible control algorithms and the absence of synchronization and reactive power. However, DC-MGs are prone to instability issues associated with the presence of nonlinear loads such as constant power loads (CPL) known by their incremental negative impedance (INI), which may lead to voltage collapse of the main DC Bus. In this paper, H_{∞} -based controller of a source side buck converter is designed to avoid the instability issues caused by the load-side converter acting as a CPL. Besides, the proposed controller allows a perfect rejection of all perturbations that may arise from parameter variations, input voltage and CPL current fluctuations. The design process of H_{∞} -based controller is based on the Golver Doyle Optimization Algorithm (GDOA), which requires an augmented system extracted from the small-signal model of the DC/DC converter including the mathematical model of parameter variations and overall external perturbations. The H_{∞} based controller involves the use of weight functions in order to get the desired performances. The proposed controller is easy to implement and lead to reducing the implementation cost and avoid the use of current measurement that may have some disadvantages. The derived controller is validated by simulation performed in Psim software and experimental setup.

Keywords: Constant Power Load, Golver Doyle Optimization Algorithm, Weight Functions, DC Microgrid, Augmented System, Structured Uncertain Parameter.

Acronyms and nomenclatures

V_{in} : Input Voltage.

\tilde{v}_{in} : Input Voltage Small Signal Value.

V_{in} : Input Voltage Nominal Value.

d : Duty Cycle.

\tilde{d} : Duty Cycle Small Signal Value.

D : Duty Cycle Nominal Value.

- 30 L : Inductance.
- 31 L_0 : Inductance Nominal value.
- 32 C : Capacitance.
- 33 C_o : Capacitance Nominal Value.
- 34 v_o : Output Voltage.
- 35 \tilde{v}_o : Output Voltage Small Signal Value.
- 36 V_o : Output Voltage Nominal Value.
- 37 i_L : Inductor Current.
- 38 \tilde{i}_L : Inductor Current Small Signal Value.
- 39 I_l : Inductor Current Nominal Value.
- 40 i_o : CPL Current.
- 41 \tilde{i}_o : CPL Current Small Signal Value.
- 42 I_o : CPL Current Nominal Value.
- 43 R_{CPL} : Incremental Negative Impedance.
- 44 P_{CPL} : Constant Power Consumed By CPL.
- 45 R : Resistance Load.
- 46 V_{ref} : Voltage Reference.
- 47 k_p : Proportional Gain of PI Controller.
- 48 k_i : Integral Gain Of PI Controller.
- 49 k_{p_v} : Proportional Gain Of Voltage PI Controller.
- 50 k_{i_v} : Integral Gain Of Voltage PI Controller.
- 51 k_{p_c} : Proportional Gain Of Current PI Controller.
- 52 k_{i_c} : Integral Gain Of Current PI Controller.
- 53 s : Laplace Variable.

- 54 $Z_1(s), Z_2(s)$: Impedance.
- 55 $M_v(s)$: Input Voltage-To-Output Voltage Transfer Function.
- 56 $Z_o(s)$: Output Impedance.
- 57 $T_p(s)$: Duty Cycle-To-Output Voltage Transfer Function.
- 58 $T_{p_o}(s)$: Duty Cycle-To-Output Voltage Nominal Transfer Function.
- 59 $\Delta(s)$: Uncertain Transfer Matrix.
- 60 $P(s)$: Augmented System.
- 61 $K_\infty(s)$: H_∞ Based Controller.
- 62 $W_1(s), W_2(s), W_3(s)$: Wight Functions.
- 63 $F_L(.,.)$: Lower Fractional Transformation.
- 64 $S(s), T(s)$: Sensibility Functions.
- 65 $\|\cdot\|_\infty$: H_∞ Norm.
- 66 \mathcal{E} : Steady-State Error.
- 67 G_m : Gain Margin.
- 68 ω_c : Cutoff Frequency.
- 69 A : System Matrix.
- 70 $C = [C_1 \ C_2]$: Output Matrix.
- 71 $B = \begin{bmatrix} B_1 \\ B_2 \end{bmatrix}$: Input Matrix.
- 72 $D = \begin{bmatrix} D_{11} & D_{12} \\ D_{21} & D_{22} \end{bmatrix}$: Feedforward Matrix.
- 73 **CPL**: Constant Power Load.
- 74 **DC**: Direct Current.
- 75 **GDOA**: Golver Doyle Optimization Algorithm.
- 76 **MG**: Microgrid.
- 77 **RES**: Renewable Energy Source.

- AC:** Alternative Current.
- INI:** Incremental Negative Impedance.
- MPC:** Model Predictive Control.
- NDO:** Nonlinear Disturbance Observer.
- PBC:** Passivity-Based Control.
- H_∞ :** H Infinity Norm.
- PWM:** Pulse Width Modulator.
- PI:** Proportional Integral Controller.
- PI_v :** Voltage PI Controller.
- PI_c :** Current PI Controller.
- RHP:** Right Half Pole-Zero Plane.
- LHP:** Left Half Pole-Zero Plane.
- VNI:** Virtual Negative Inductance.
- MPC:** Model Predictive Control.
- SMC:** Sliding Mode Control.

1. Introduction

Over the past decade, industrialized countries have actively promoted the liberalization of the electricity market, as well as the promotion of the integration of the principles of energy efficiency and renewable energies in the supply and consumption of electricity [1]. This transition is considered to be a trend, which implies the reduction of the environmental impact associated with the centralized production of electricity based on fossil fuels, the reduction of greenhouse gas emissions and the mutation from centralized to distributed generation by the integration of renewable energy sources (RESs) which improve the overall efficiency of the electrical system [2]. In the context of distributed generation, the concept of microgrids (MGs) arises. A MG is an electrical system consisting of distributed and interconnected generators, loads and distributed units of electrical energy storage that cooperate with each other by acting collectively as a single consumer or producer system. System coordination includes coordination of control and protection devices as well as energy management and intelligent control functionalities [1-2]. Fig. 1 depicts the DC-MG configuration.

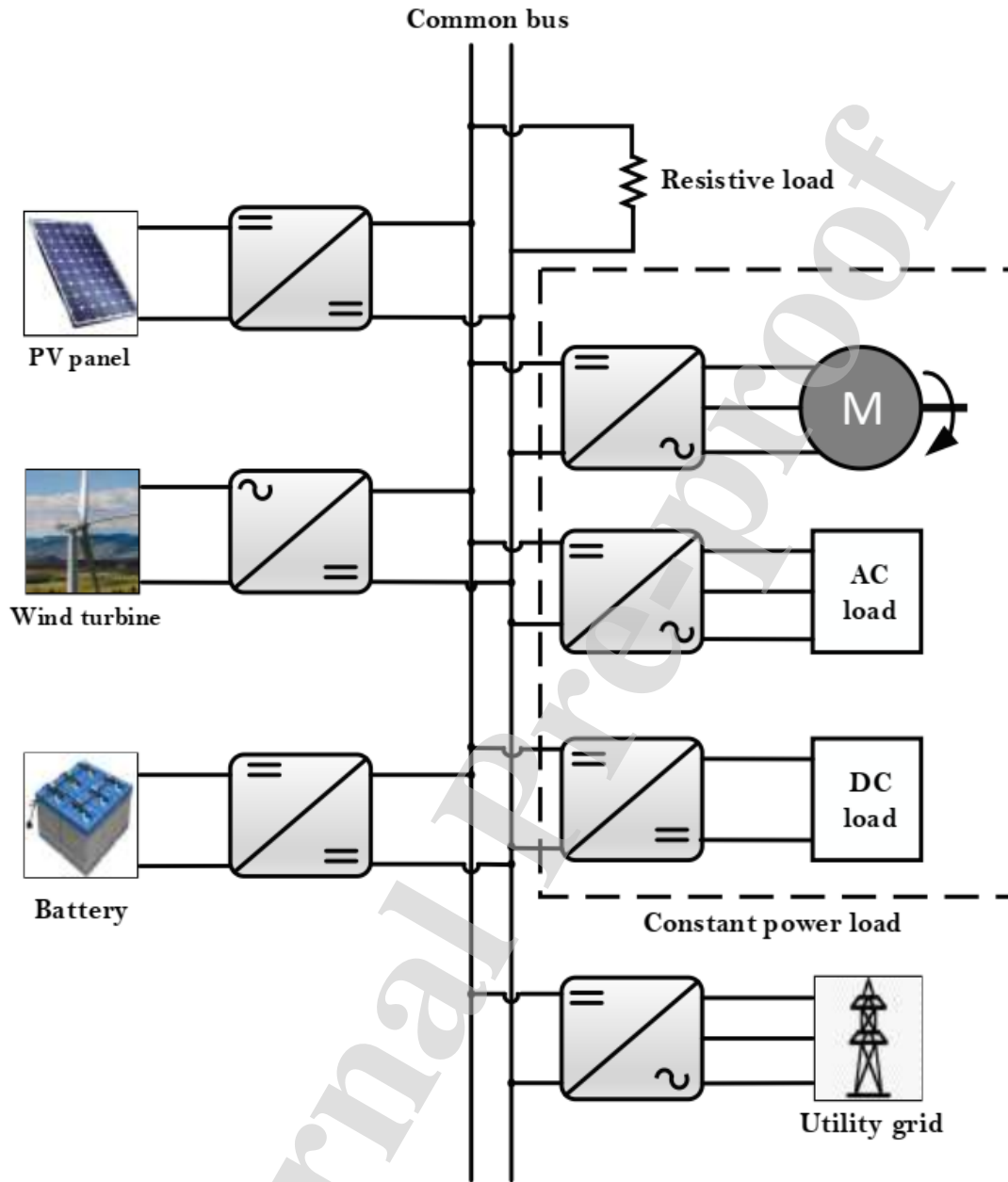


Fig. 1. DC-MG configuration.

MG architecture can be classified into three types: AC-MG, DC-MG and hybrid AC/DC-MG [3-4]. It can operate in grid-connected mode or islanded mode [5-9]. From the point of view of energy efficiency, ease of control and reliability, DC-MGs are gaining more and more interest compared to AC-MG. On the other hand, as the number of DC-generating RESs is higher as compared to AC-generating sources, lesser converter units are required. Also, harmonic issues and synchronization needed in AC-MG do not arise in DC-MG. The storage

devices play an important role in DC-MG, which is providing the power balance and bus stability [10].

However, DC-MG is prone to instability issues. These instability issues are often associated with the presence of Constant Power Loads (CPL) in the microgrids [11-23]. This type of load refers to the one that is controlled such as a load converter whose output voltage is firmly regulated to feed a passive load [14], [15]. These loads include a power converter that regulates their voltages such that the whole regulated system appears as drawing a constant power [18].

The CPL is a nonlinear load with incremental negative impedance (INI) characteristic [23], which implies the load current increase/decrease with the decrease/ increase in its terminal voltage. DC-MG may become unstable when it feeds the CPL, which generates the oscillations in the system that may cause the stress and failures in the MG equipment [16], [19]. For this reason, the CPL issue has attracted more intention of researchers to find appropriate control methods in order to avoid CPL instability issues [12]. In addition, the perturbations brought by the load current and DC source voltage and the variations of system parameters may lead to losing system performances [21]. On the other hand, the system stability is not guaranteed as it can be completely lost when substantial parameter variation occurs in one of the physical components of the system under control based on the conventional controllers [22].

To solve the aforementioned issues, traditional methods based on conventional controllers can be ineffective [23]. Thus, many control methods have been proposed in the literature. The first proposed method is the passive damping. It consists of adding passive components to the DC/DC converter in order to increase the damping factor [24-29]. For instance, in [24], the authors proposed a specific technique based on a simplified system representation consisting of a voltage source, an LC filter and ideal CPL for choosing the necessary passive components. In [25], the authors proposed a stabilizer device, which consists of an additional battery connected to DC Bus through a DC/DC converter operating under a specific control. However, this approach decreases the system efficiency by causing excessive power losses.

An active damping approach is proposed by many authors. It consists of adding a virtual impedance to modify the closed-loop control that lets the system poles lying on the LHP [30-35]. For instance, in [30], the authors proposed the virtual impedance consisting of series-connected resistance and inductance. In [31], the authors proposed a virtual resistance

associated with an additional output voltage feedback loop. In [34], a feedforward technique aiming to create a virtual R-C filter at the input of the CPL is proposed. In [35], the virtual negative inductance (VNI) depending on the CPL current estimated by the nonlinear disturbance observer (NDO) is investigated. This approach is effective to ensure the system stability in different cases with the presence of CPL. However, the original converter control loop will be modified and consequently the dynamic response of the overall system will be affected.

Taking into account the nonlinearity of the DC/DC converter, nonlinear control techniques have been implemented to stabilize the DC-MG feeding CPLs. Among them, model predictive control (MPC) has been proposed by many authors [37-42]. For instance, in [37] the possibility of applying a finite control set model predictive control (FCS-MPC) algorithm for dynamic stabilization of DC-MG supplying CPL is studied. In [38] and [39], the authors investigated the fuzzy model predictive control synthesis of networked controlled power buffer for dynamic stabilization of a DC-MG supplying CPL. The proposed approach is based on Takagi-Sugeno (TS) fuzzy model and model predictive scheme. This approach is effective to overcome CPL instability issues. But, MPC is not suitable for plant-wide in real-time, due to its computational burden [42]. The Sliding Mode Control (SMC) has been also proposed to enhance the system stability [43-48]. Authors in [46] proposed a novel sliding manifold that results in stable operation for a wide range of gains, followed by rigorous stability condition analysis to reach a suitable enhancement of the closed-loop system dynamic response. In [47], the authors have proposed a digital sliding mode control (DSMC) for a boost converter under CPL conditions. However, the sliding mode approach requires the capacitor current measurement, which causes ripple filtering degradation with the apparition of the shattering problem [49].

Backstepping and passivity based control are one of the most nonlinear control design tools to avoid the instability caused by INI characteristic and to solve the tracking problem [21], [36], [50-52]. For instance, in [36] and [50], the authors proposed the backstepping control with integrating NDO and 3rd-degree Cubature Kalman filter (CKF) respectively. In [21], the instability due to CPL is avoided by applying the passivity-based control (PBC) through integrating the NDO observer. In papers [51] and [52], the authors proposed an improvement of Interconnection and Damping Assignment Passivity-Based Control (IDA-PBC) by developing an interconnection matrix to elaborate the internal link in port-controlled Hamiltonian (PCH) models.

The methods mentioned in the literature target one objective presented in stabilizing the DC-MG supplying CPL. Their implementations might be difficult and costly, may require a large use of sensors and introduce the use of passive elements that reduce the system efficiency. This paper proposes H_∞ based-controller of a source side buck converter whose implementation is easy and require only one sensor of voltage measurement. The proposed controller increases the damping factor of system without using the passive elements aiming to reach three objectives given below:

- 1) Avoiding the system instability caused by the load-side converter acting as CPL.
- 2) Rejecting all perturbations that arise from the parameter variations, input voltage and current fluctuations.
- 3) Implementation of the derived control strategy in low cost DSP.

The H_∞ based-controller process design is based on Golver Doyle Optimization Algorithm (GDOA), which requires an augmented system extracted from the small-signal model of DC/DC converter including the mathematical model of overall external perturbations that may arise from parameter variations, input voltage and CPL current fluctuations. The use of the weight functions included in the augmented system is required by the design process in order to obtain desired performances. The proposed method is validated by simulation performed in Psim software and experimental setup.

This paper is organized as follows: Section 2 describes the system configuration and problem statement. Section 3 and section 4 present the modeling of a buck converter with uncertain parameters and considering the overall exiting perturbations. Section 5 investigates the design process of the H_∞ based-controller and section 6 analyses the stability conditions. The H_∞ based controller effectiveness is validated by both simulation and experimental setup in sections 7 and 8. The paper is ended with a conclusion.

2. System configuration and problem statement

As mentioned previously, converters with tightly regulated output act as CPL. In this paper, we consider a buck converter operating in continuous conduction mode (CCM) feeding a resistive load via a voltage controlled boost converter as depicted in Fig. 2 (a). The equivalent circuit of the load side converter is shown in Fig. 2 (b) where it is replaced by a controlled current source [36].

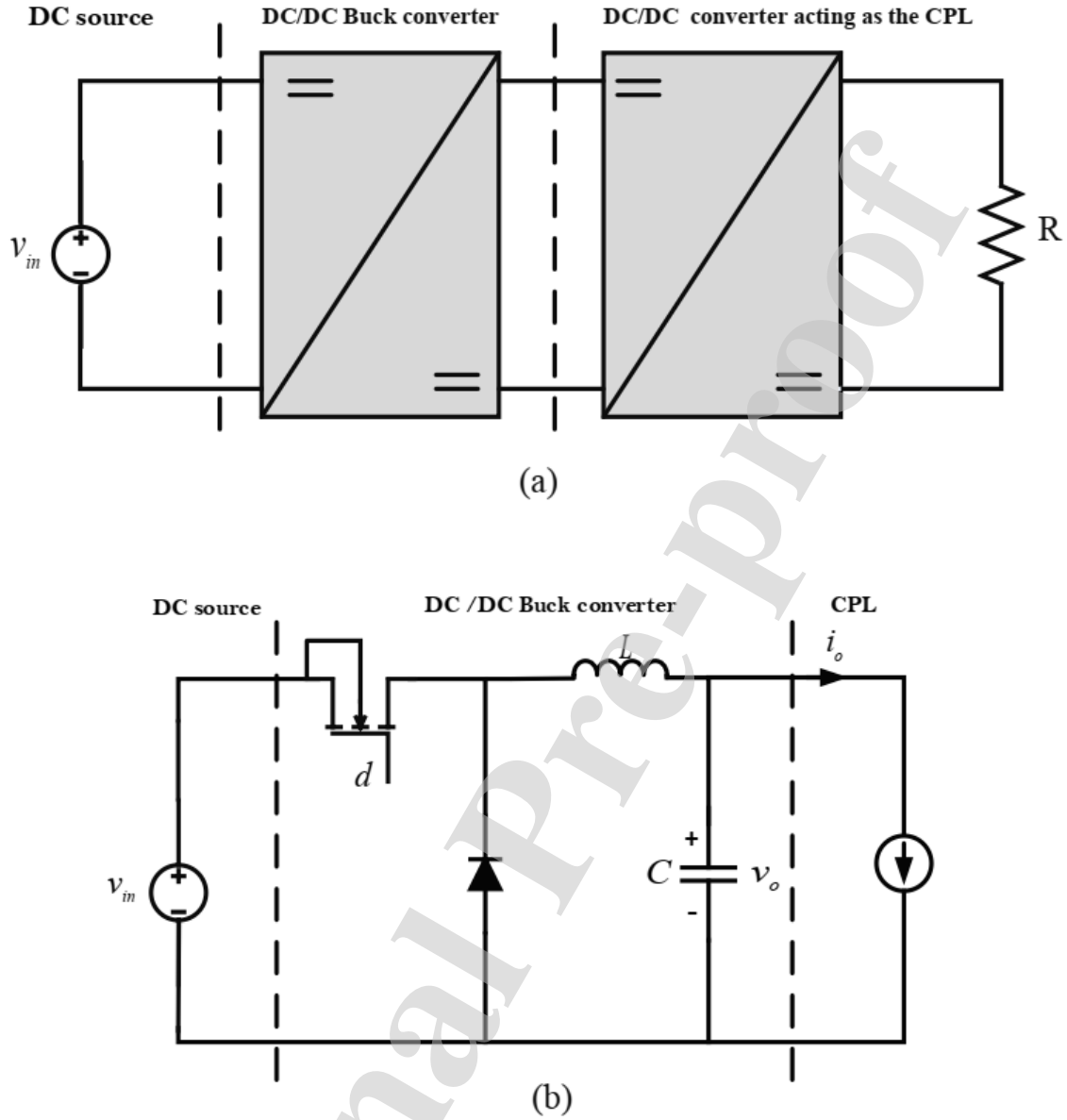


Fig. 2. Configuration of DC/DC buck converter feeding CPL.

For a CPL, the absorbed power within the controller bandwidth is constant and its relation is given as follows [23], [60]:

$$P_{CPL} = v_o \cdot i_o \quad (1)$$

By deriving the CPL current with respect to its voltage, the expression of the incremental negative impedance (INI) of the CPL is obtained as follow:

$$R_{CPL} = \frac{dv_o}{di_o} = -\frac{P_{CPL}}{i_o^2} = -\frac{v_o}{i_o} = -\frac{v_o^2}{P_{CPL}} \quad (2)$$

According to equation (2), the CPL presents has incremental negative impedance (INI) characteristic, which presents 180° phase lag in the bode diagram. Therefore, when cascading with a source converter, if the output impedance module of the source converter intersects with the CPL input impedance module, instability arises [63]. To avoid the negative effect of INI characteristic and increasing the damping factor of the overall system, a passive load is usually connected to the common DC bus. In general, the passive load can be a resistive load or an additional stabilizer device [24], [29]. However, this component inherently causes power loss. Thus, the system operates at low efficiency. To illustrate the aforementioned issues, Fig. 3 and Fig. 4 show simulation results of the INI characteristic effect on the output voltage and the ability of the additional resistive load to avoid the corresponding oscillations.

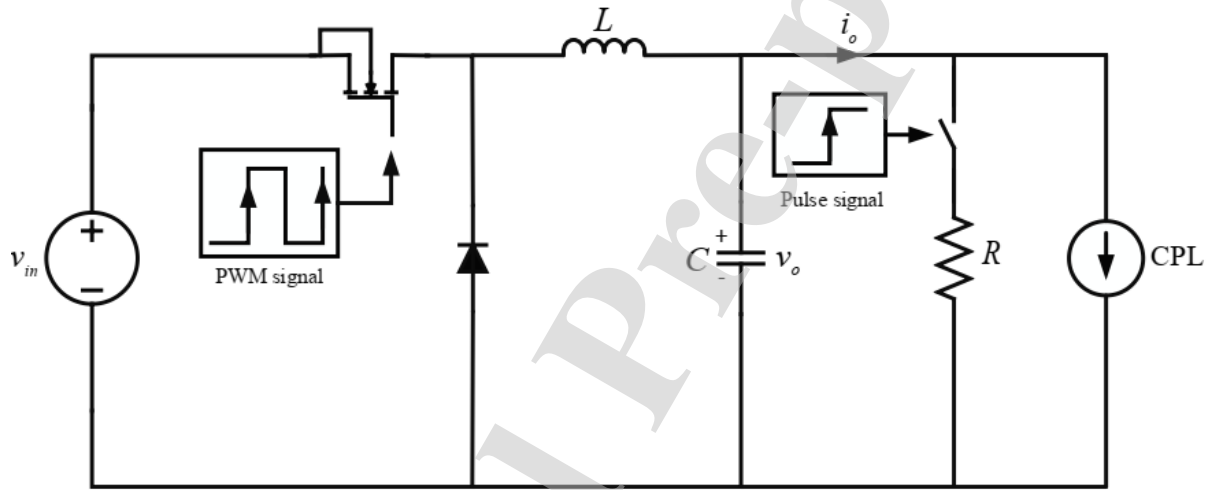


Fig. 3. Buck converter feeding a CPL and a damping resistor

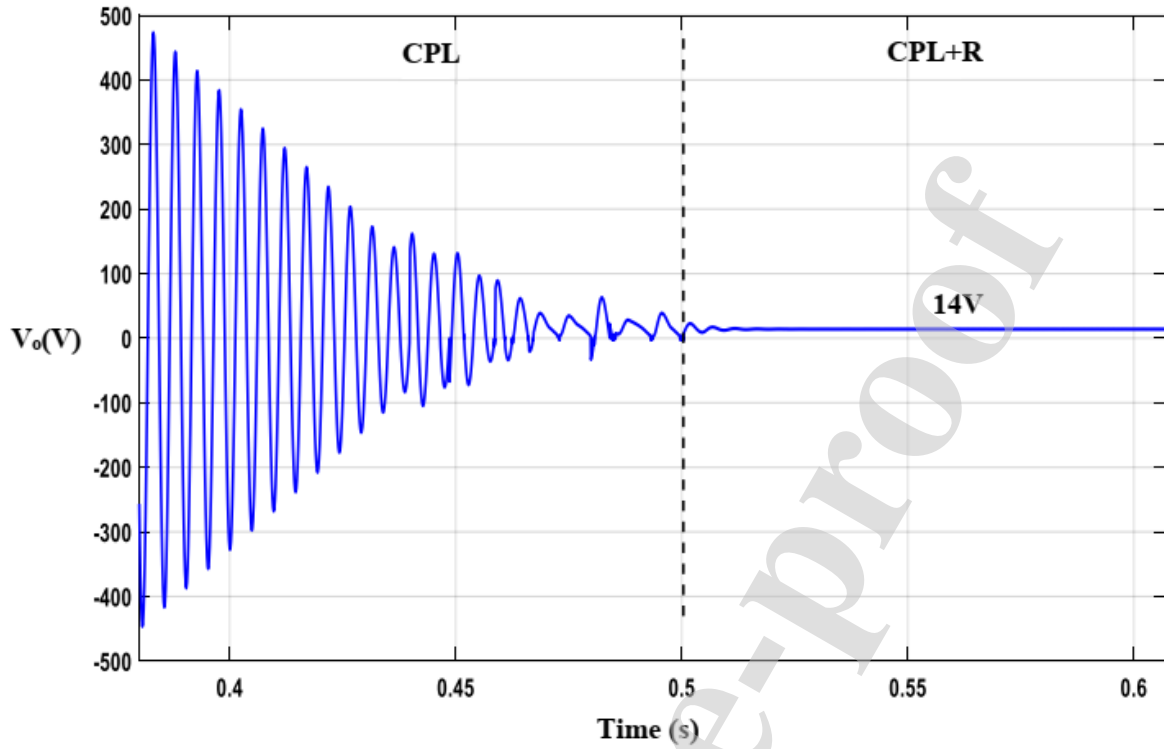
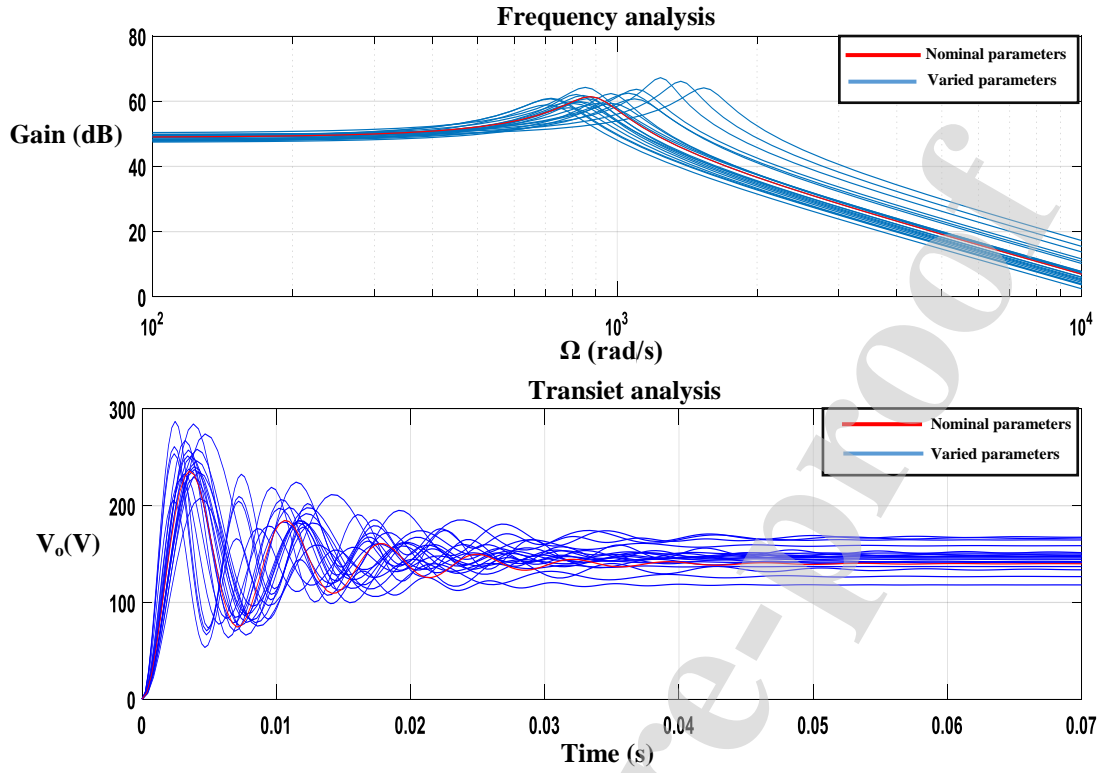


Fig. 4. Ability of passive load to mitigate the oscillation of output voltage caused by CPL ($v_{in} = 25V$, $D = 0.5$, $C = 220\mu F$, $L = 2.7mH$, $R_{CPL} = -9.8\Omega$, $P_{CPL} = 20W$, $R = 5\Omega$).

In addition, parameter variations might deteriorate the system performances such as the settling time and overshoot. To understand the corresponding problem, transient and frequency analysis of the system with a damping resistor are depicted in Fig. 5. The parameter variations influence negatively the cut-off frequency and quality factor that brings to the system a substantial overshoot and slow transit dynamic.



236

Fig. 5. Transient and frequency analysis of the studied system ($(470 - 30\%) < C < (470 + 30\%)$, $(2.7 - 60\%) < L < (2.7 + 60\%)$, $D = 0.5$, $v_o = 140V$, $v_{in} = 280V$, $P_{CPL} = 20W$, $R = 5\Omega$).

237

238 Fig. 6 and Fig. 7 show the instability occurred when the output capacitance value tolerates.

239 The converter is controller using conventional PI controller.

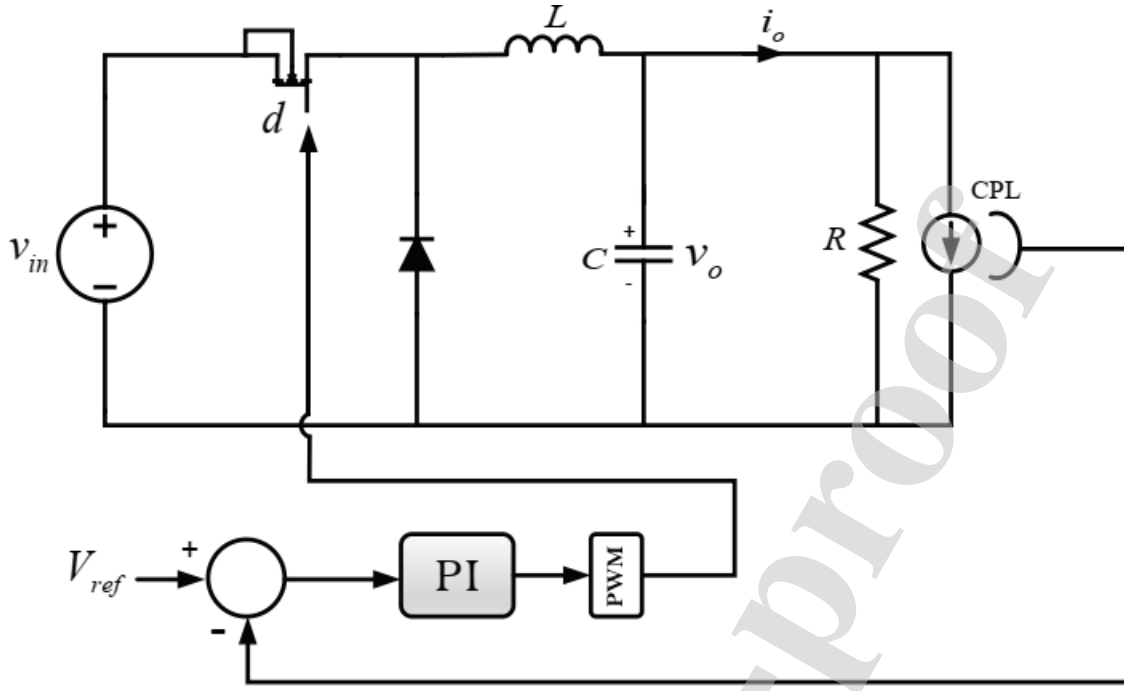


Fig. 6. Buck converter feeding a mixed load under conventional PI control.

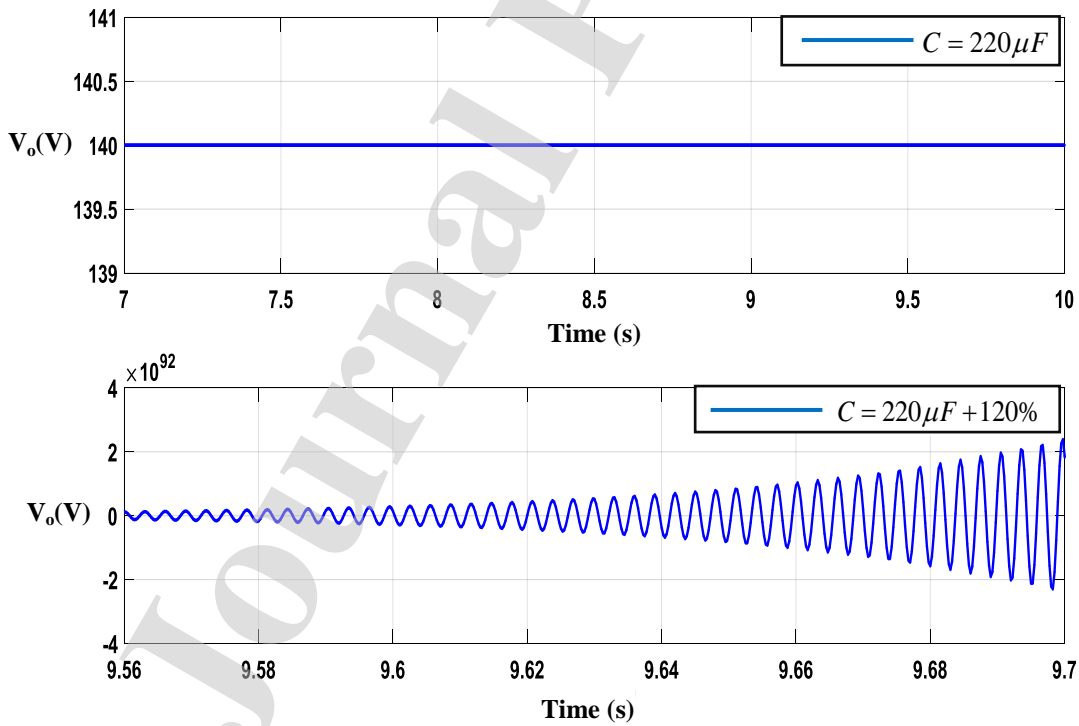


Fig. 7. Step response of the studied system under capacitance variation ($L=2.7mH$, $v_{in}=280V$, $v_o=140V$, $R=5\Omega$, $R_{CPL}=-9.8\Omega$, $k_p=0.0158$, $k_i=4.965$).

In Addition, the PI controller and conventional cascade control are ineffective for maintaining the stability of the system feeding CPLs [23]. Fig. 8 and Fig. 9 shows a simulation study of a DC/DC buck converter feeding the CPL operating under conventional cascade control and the instability caused by the increase of CPL demanded-power.

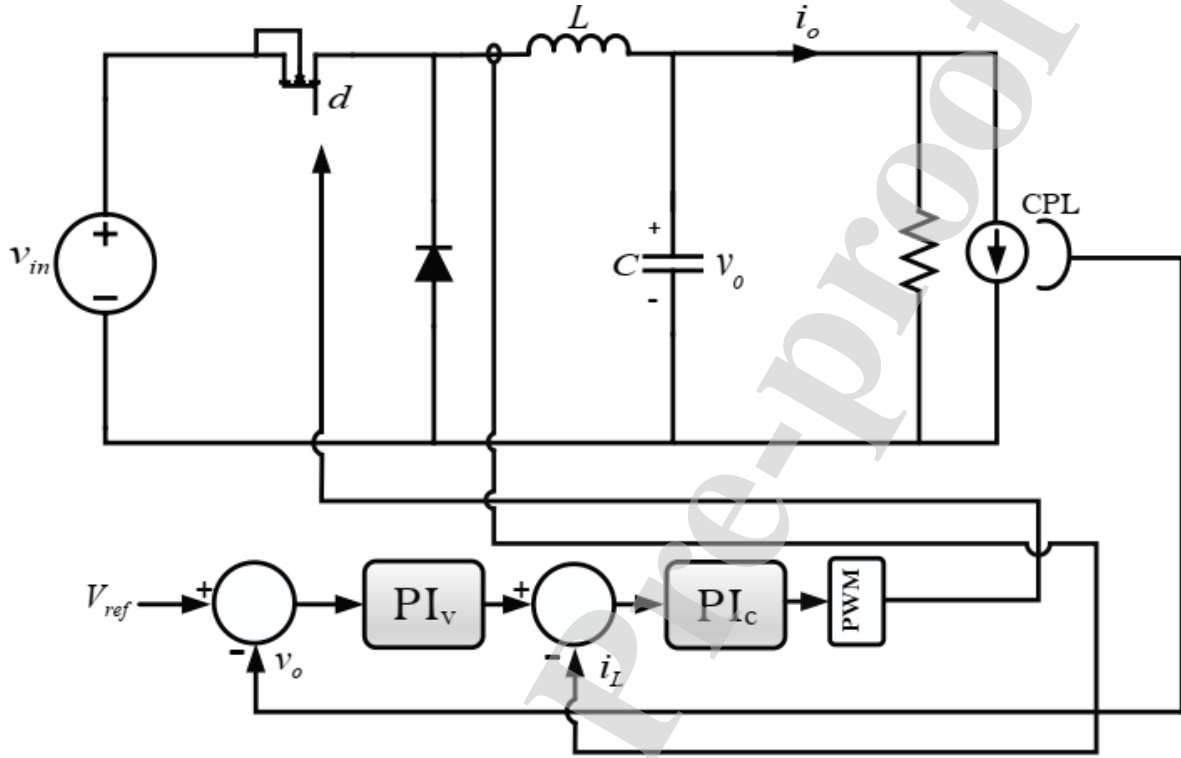


Fig. 8. Buck converter feeding a CPL operating under conventional cascade control.

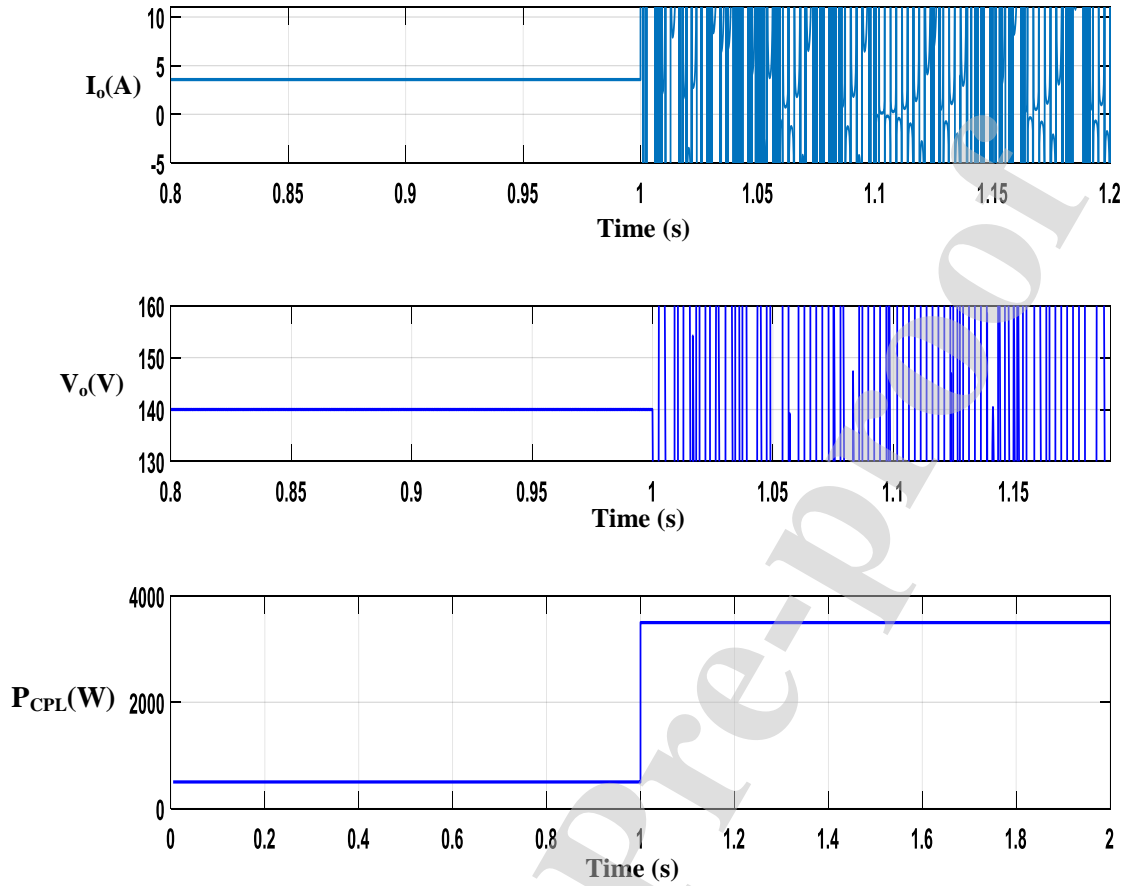


Fig. 9. Effect of the increase of CPL demanded power on the system operation under conventional cascaded control ($L=2.5mH$, $C=220\mu F$, $v_{in}=280V$, $v_o=140V$, $k_{p_v}=2.5$, $k_{i_v}=1.501 \cdot 10^4$, $k_{p_c}=0.003375$, $k_{i_c}=1$).

The main purpose of the present work is to achieve a stable operation of the DC-MG under CPL condition without using the passive loads. The proposed control strategy also aims to reject all perturbations brought by the parameter variations, input voltage and load fluctuations. In the following sections, system modelling, controller process design and stability analysis are investigated.

3. System modeling

The basic of control design of a DC/DC converter passes through system modeling, which allows describing CPL behavior. To this end, the small-signal method is chosen to model the buck converter feeding the CPL [60], [61]. The small-signal model equivalent circuit of the studied system is depicted in Fig. 10.

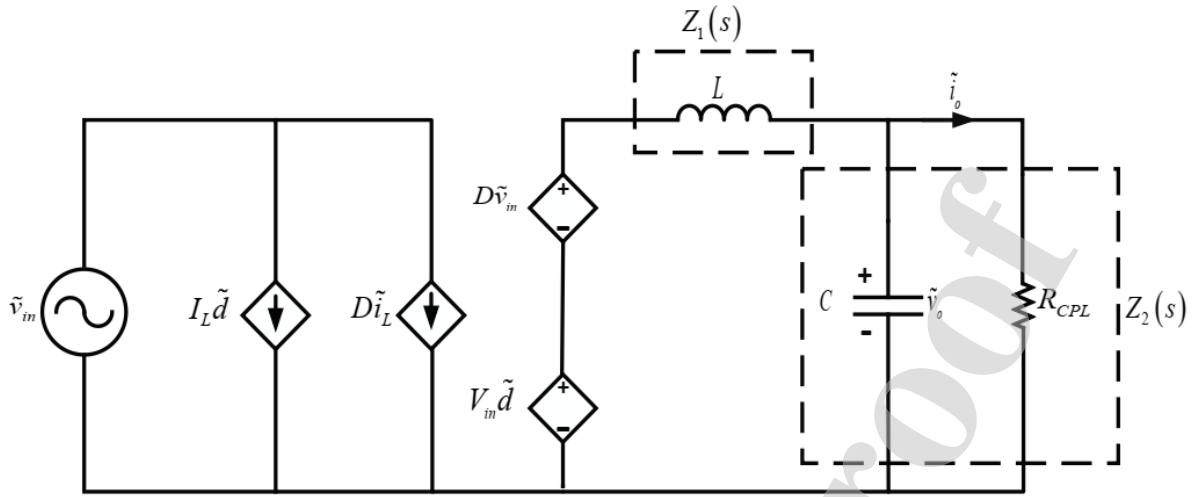


Fig. 10. Equivalent circuit of buck converter feeding CPL.

The system is considered as multi-inputs single-output (MISO) involving three input variables, namely: the duty cycle \tilde{d} that is the control variable, the CPL current \tilde{i}_o and the input voltage. While the output variable is the output voltage \tilde{v}_o . It is worth to point out that the CPL current \tilde{i}_o and the input voltage \tilde{v}_{in} are considered as external perturbations.

According to the equivalent circuit given in Fig. 10, the transfer functions that link the input variables to the output variable are depicted in Fig. 11 [61]:

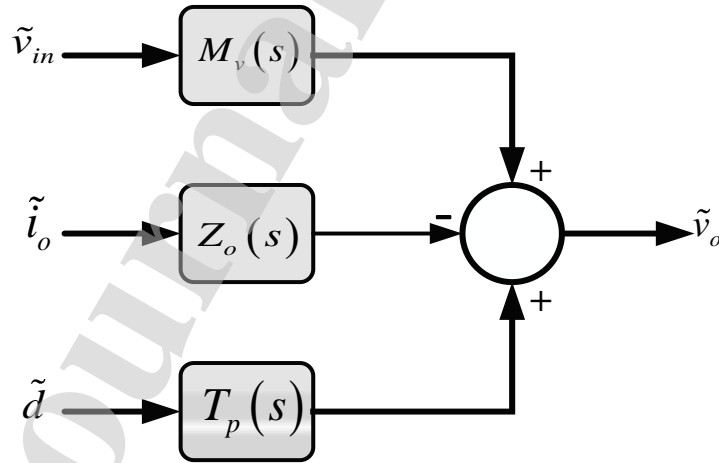


Fig. 11. Block diagram of buck converter open-loop transfer function.

Their corresponding mathematical expressions are given below:

$$T_p(s) = \left. \frac{\tilde{v}_o(s)}{\tilde{d}(s)} \right|_{\tilde{v}_{in}=0} = \frac{V_{in}Z_2(s)}{Z_1(s) + Z_2(s)} = \frac{\frac{V_{in}}{LC}}{s^2 - \frac{P_{CPL}}{CV_o^2}s + \frac{1}{LC}} \quad (3)$$

$$M_v(s) = \left. \frac{\tilde{v}_o(s)}{\tilde{v}_{in}(s)} \right|_{\tilde{d}=0} = \frac{DZ_2(s)}{Z_1(s) + Z_2(s)} = \frac{\frac{D}{LC}}{s^2 - \frac{P_{CPL}}{CV_o^2}s + \frac{1}{LC}} \quad (4)$$

$$Z_o(s) = \frac{Z_1(s)Z_2(s)}{Z_1(s) + Z_2(s)} = \frac{\frac{s}{C}}{s^2 - s\frac{P_{CPL}}{CV_o^2} + \frac{1}{LC}} \quad (5)$$

278 where

$$Z_1(s) = sL \quad (6)$$

$$Z_2(s) = \frac{R_{CPL} \frac{1}{Cs}}{R_{CPL} + \frac{1}{Cs}} \quad (7)$$

279

280 According to equation (3), the INI characteristic of the CPL brings to the system two complex
 281 conjugate poles in the RHP of the pole-zero plane. Fig. 12 shows the impact of INI
 282 characteristic on the poles evolution of the mathematical model of buck converter feeding the
 283 CPL.

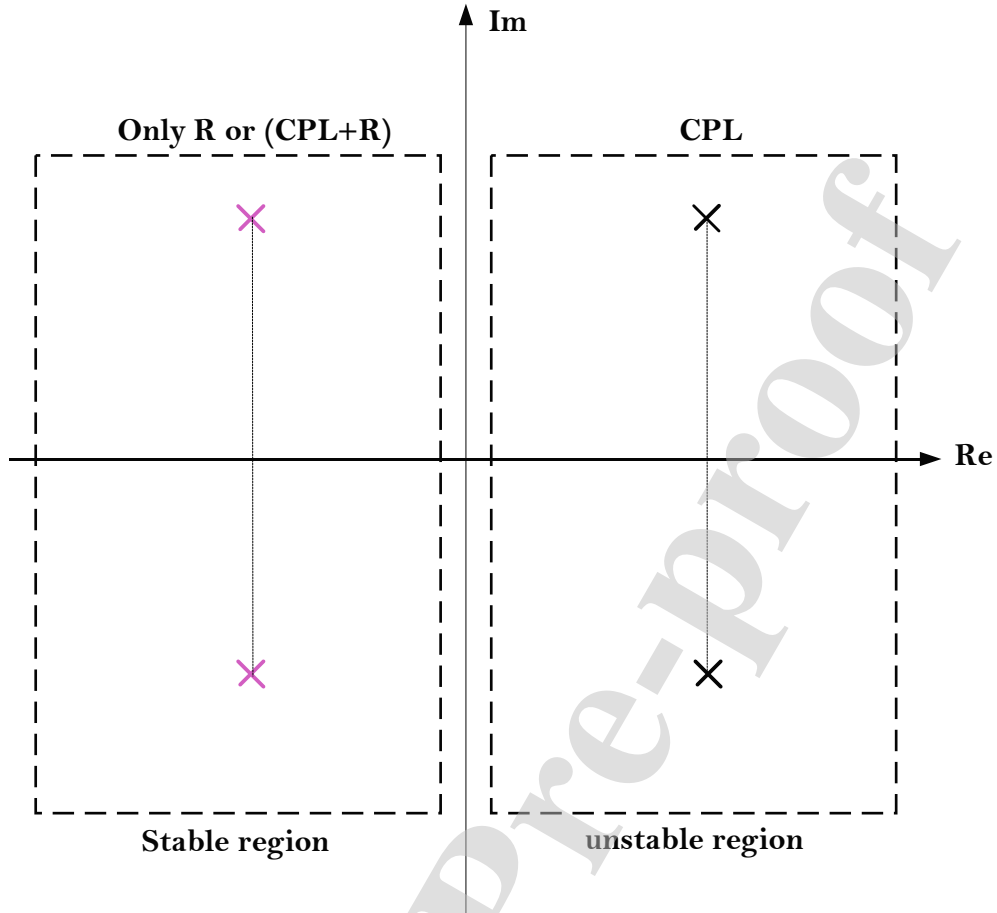


Fig. 12. Impact of CPL load on the poles evolution of buck converter model.

To ensure the robustness for the system against the parameter variations, the process of the control design requires an uncertain model of system to design a controller that will have the robustness against all of the aforementioned issues. This type of modeling consists of introducing the mathematical model of parameter variations and whole external perturbations. It will be investigated in the next section.

4. Uncertain system modelling:

Parameter variations are considered as structured uncertainties [62], which are defined as follows:

Definition 1:

Assuming Ψ is an uncertain parameter such as:

$$\Psi = \Psi_0 + \Psi_0 \delta_\Psi \quad (9)$$

where, Ψ_0 is the nominal value and δ_Ψ is the random parameter that takes different values.

298 Based on this definition 1, the parameters of the transfer function (3) will have the following
 299 expressions:

$$\begin{cases} \frac{V_{in}}{LC} = b & b = b_0 + \delta_b \cdot b_0 & b_0 = \left(\frac{V_{in}}{LC} \right)_0 = \frac{V_{in}}{L_0 C_0} \\ \frac{P_{CPL}}{CV_o} = k & k = k_0 + \delta_k \cdot k_0 & k_0 = \left(\frac{P_{CPL}}{CV_o} \right)_0 = \frac{P_{CPL}}{V_o C_0} \\ \frac{1}{LC} = \theta & \theta = \theta_0 + \delta_\theta \cdot \theta_0 & \theta_0 = \left(\frac{1}{LC} \right)_0 = \frac{1}{L_0 C_0} \end{cases} \quad (10)$$

300 Substituting each parameter of (3) by the corresponding mathematical expression given in
 301 (10) and supposing $\tilde{v}_{in} = \tilde{i}_o = 0$, the output variable \tilde{v}_o is given as follows:

$$\tilde{v}_o = \frac{b_0}{s^2 - s \cdot \theta_0 + k_0} \tilde{d} + \frac{b_0 \delta_b \tilde{d} + (\theta_0 \delta_\theta s - k_0 \delta_k) \tilde{v}_o}{s^2 - s \theta_0 + k_0} \quad (11)$$

302 After some mathematical manipulations, the output variable \tilde{v}_o will be expressed as:

$$\tilde{v}_o = (\omega + \tilde{d}) \overbrace{\frac{b_0}{s^2 - \theta_0 s + k_0}}^{T_{p0}(s)} \quad (12)$$

303 where ω is the variable that acts as an internal perturbation and given by the following
 304 expression:

$$\omega = \overbrace{\frac{1}{T_{p0}(s)} \cdot \left[\frac{b_0 \delta_b}{s^2 - \theta_0 \cdot s + k_0} - \frac{\theta_0 \delta_\theta s - k_0 \delta_k}{s^2 - \theta_0 \cdot s + k_0} \right]}^{\Delta(s)} \cdot \begin{pmatrix} \tilde{d} \\ \tilde{v}_0 \end{pmatrix} \quad (13)$$

305 In the case of $\tilde{v}_{in} \neq \tilde{i}_o \neq 0$, the output variable \tilde{v}_o is expressed as:

$$\tilde{v}_o = (\omega + \tilde{d}) T_{p0}(s) + Z_o(s) \tilde{i}_o + M_v(s) \tilde{v}_{in} \quad (14)$$

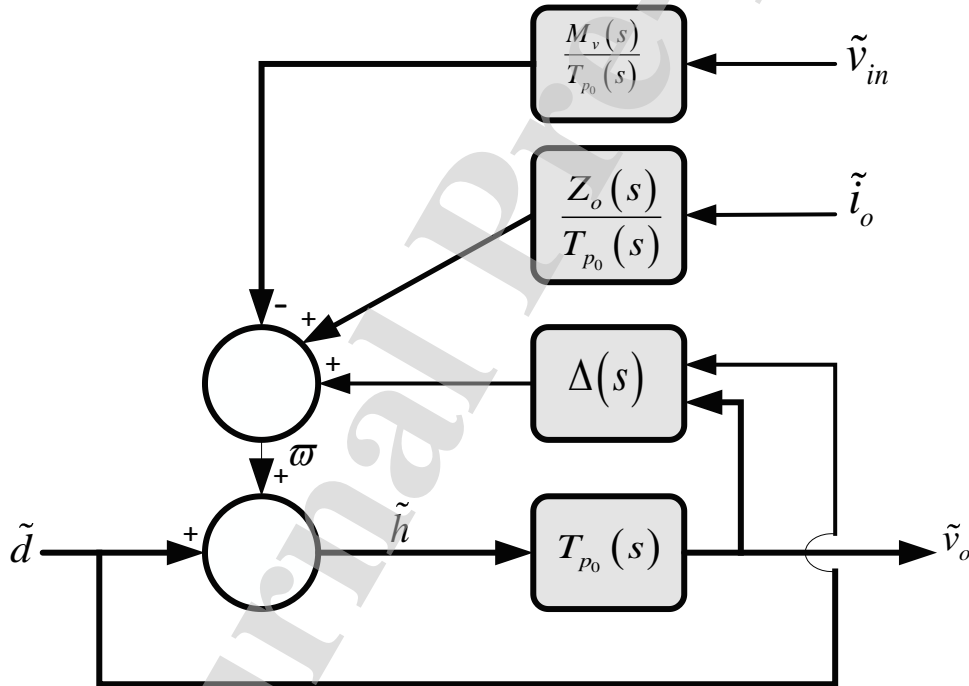
306 and also can be expressed as:

$$\tilde{v}_0 = \left(\tilde{d} + \omega + \frac{Z_0(s)}{T_{p_0}(s)} \tilde{i}_0 + \frac{M_v(s)}{T_{p_0}(s)} \tilde{v}_{in} \right) T_{p_0}(s) \quad (15)$$

307 Denoting that: ω is the sum of perturbations and influence on the actual control action. Its
 308 mathematical expression is given as follows:

$$\omega = \omega + \frac{Z_0(s)}{T_{p_0}(s)} \tilde{i}_0 + \frac{M_v(s)}{T_{p_0}(s)} \tilde{v}_{in} \quad (16)$$

309 To make the system model including the overall perturbations more obvious, Fig. 13 shows
 310 the block diagram of the corresponding model including whole perturbations, which are
 311 gathered in ω , which affect negatively the actual control variable \tilde{h} .



312
 313 **Fig. 13.** The uncertain model including the external and internal perturbations.

314 5. Control design

315 In this work, GDOA is used to optimize a controller based on the H_∞ norm. This algorithm
 316 requires an augmented system that is the relationship between the variables of interest (the
 317 error and control variables) and the overall perturbations [54], [55]. The augmented system
 318 includes the weight functions that are used to construct the controller and to obtain the desired
 319 performances [56].

Fig 14 depicts the voltage closed-loop control, where $K_{\infty}(s)$ is the derived controller, $W_1(s)$, $W_2(s)$ and $W_3(s)$ are the weight functions, $y = V_{ref} - \tilde{v}_o$ is the error, $u = \tilde{d}$ is the control variable, e_1 is the error filtered by $W_1(s)$ and e_2 is the control variable filtered by $W_2(s)$.

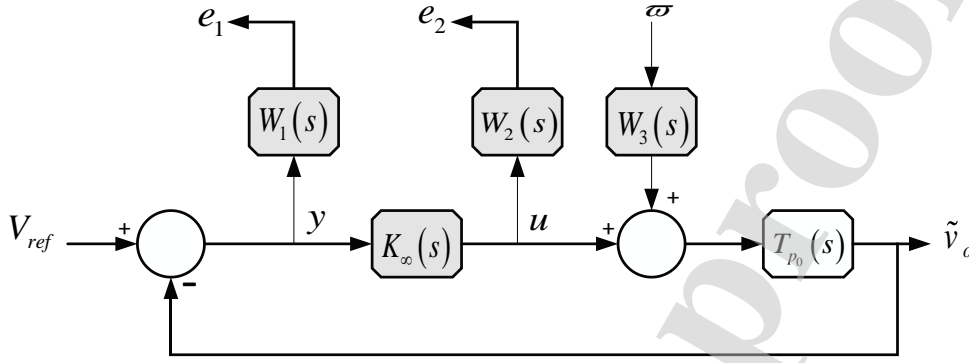


Fig. 14. Voltage robust closed-loop control.

According to voltage closed-loop control depicted in Fig. 14, the augmented system is developed as follows:

$$\begin{bmatrix} e_1 \\ e_2 \\ y \end{bmatrix} = [P(s)] \begin{bmatrix} V_{ref} \\ w \\ u \end{bmatrix} \quad (16)$$

where

$$[P(s)] = \begin{bmatrix} W_1(s) & -W_1(s)T_{p_0}(s)W_3(s) & -W_1(s)T_{p_0}(s)W_3(s) \\ 0 & 0 & W_2(s) \\ 1 & -W_3(s)T_{p_0}(s) & -T_{p_0}(s) \end{bmatrix} \quad (17)$$

and

$$u = K_{\infty}(s)y \quad (18)$$

$S(s)$ and $T(s)$ are the sensitivity functions, which are expressed as:

$$S(s) = \frac{1}{1 + K_{\infty}(s) \cdot T_{p_0}(s)} \quad (19)$$

and

$$T(s) = \frac{K_\infty(s) \cdot T_{p_0}(s)}{1 + K_\infty(s) \cdot T_{p_0}(s)} \quad (20)$$

332 considering that

$$e = \begin{bmatrix} e_1 \\ e_2 \end{bmatrix} \quad (21)$$

333 and

$$\omega_g = \begin{bmatrix} V_{ref} \\ w \end{bmatrix} \quad (22)$$

334 According to [62], the lower fractional transformation $e = F_L(P(s), K_\infty(s)) \cdot \omega_g$, which
 335 references the closed-loop transfer function matrix with considering ω_g is the inputs vector
 336 and e is the outputs vector, is given by:

$$e = \begin{bmatrix} W_1(s) & W_1(s)S(s)T_{p_0}(s)W_3(s) \\ W_2(s)S(s)K_\infty(s) & -W_2(s)T(s)W_3(s) \end{bmatrix} \cdot \omega_g \quad (23)$$

337 Based on theorem 3 (see appendix), the designed controller achieves the main objectives if the
 338 following condition is satisfied:

$$\|F_L(P(s), K_\infty(s))\|_\infty \leq \gamma \quad (24)$$

339 That gives:

$$\|S(s)\|_\infty \leq \frac{\gamma}{\|W_1(s)\|_\infty} \xrightarrow{A_1} |S(s)| \leq \overbrace{\frac{\gamma}{|W_1(s)|}}^{A_2} \quad (25)$$

$$\|S(s)T_{p_0}(s)\|_\infty \leq \frac{\gamma}{\|W_1(s)W_3(s)\|_\infty} \xrightarrow{A_3} |S(s)T_{p_0}(s)| \leq \overbrace{\frac{\gamma}{|W_1(s)W_3(s)|}}^{A_4} \quad (26)$$

$$\|S(s)K_\infty(s)\|_\infty \leq \frac{\gamma}{\|W_2(s)\|_\infty} \xrightarrow{A_5} |S(s)K_\infty(s)| \leq \overbrace{\frac{\gamma}{|W_2(s)|}}^{A_5} \quad (27)$$

$$\|T(s)\|_{\infty} \leq \frac{\gamma}{\|W_2(s)W_3(s)\|_{\infty}} \xrightarrow{A_7} |T(s)| \leq \overbrace{\frac{\gamma}{|W_2(s)W_3(s)|}}^{A_8} \quad (28)$$

340 The γ value is positive and will be extracted using GDOA. Based on [57] and [58], the
341 selected weight functions have the following mathematical expressions:

$$W_1(s) = \frac{1}{K_1} \cdot \frac{s + \omega_c K_1}{s + \omega_c k_1} \quad (29)$$

$$W_2(s) = \frac{1}{k_2} \cdot \frac{s + \frac{\omega_c}{K_2}}{s + \frac{\omega_c}{k_2}} \quad (30)$$

342 and

$$W_3(s) = K \quad (31)$$

343 The parameters of the selected weight functions are given as follows:

$$K_1 = K_2 = e^{\frac{-\log(10)G_m}{20}} \quad (32)$$

$$k_1 = k_2 = \varepsilon \quad (33)$$

344 and

$$K \ll \varepsilon \quad (34)$$

345 Where ε is the steady-state error, G_m and ω_c are the gain margin and cutoff frequency for
346 desired performances respectively. It is worth mentioning here that there are no unique
347 mathematical expressions of the selected weight functions.

348 The state-space representation $P(s)$ is given as follows:

$$[P(s)] = \left[\begin{array}{c|cc} \underline{A} & \underline{B}_1 & \underline{B}_2 \\ \hline C_1 & D_{11} & D_{12} \\ C_2 & D_{21} & D_{22} \end{array} \right] \quad (35)$$

349 where,

$$\begin{cases} \dot{x} = Ax + B_1 \begin{bmatrix} V_{ref} \\ \varpi \end{bmatrix} + B_2 u \\ e = C_1 x + D_{11} \begin{bmatrix} V_{ref} \\ \varpi \end{bmatrix} + D_{12} u \\ y = C_2 x + D_{21} \begin{bmatrix} V_{ref} \\ \varpi \end{bmatrix} + D_{22} u \end{cases} \quad (36)$$

350 According to (36) and based on theorems 1, 2 and 3 (see appendix), the robust controller is
 351 derived as follows:

$$[K_\infty(s)] = \begin{bmatrix} \hat{A}_\infty & | & Z_\infty Y_\infty C_2^* \\ -B_2^* & | & 0 \end{bmatrix} \quad (39)$$

352 where,

$$K_\infty(s) = -B_2^* (sI_n - \hat{A}_\infty)^{-1} Z_\infty Y_\infty C_2^* \quad (38)$$

353 Where I_n is the identity matrix and n is the order of the controller.

354 The developed algorithm of GDOA is performed under Matlab software. It starts with an
 355 initial value γ and will stop at the final value when the conditions (24) is satisfied. Besides, it
 356 is necessary to verify the conditions (25-28). Fig. 15 shows a summary of GDOA represented
 357 by the flowchart.

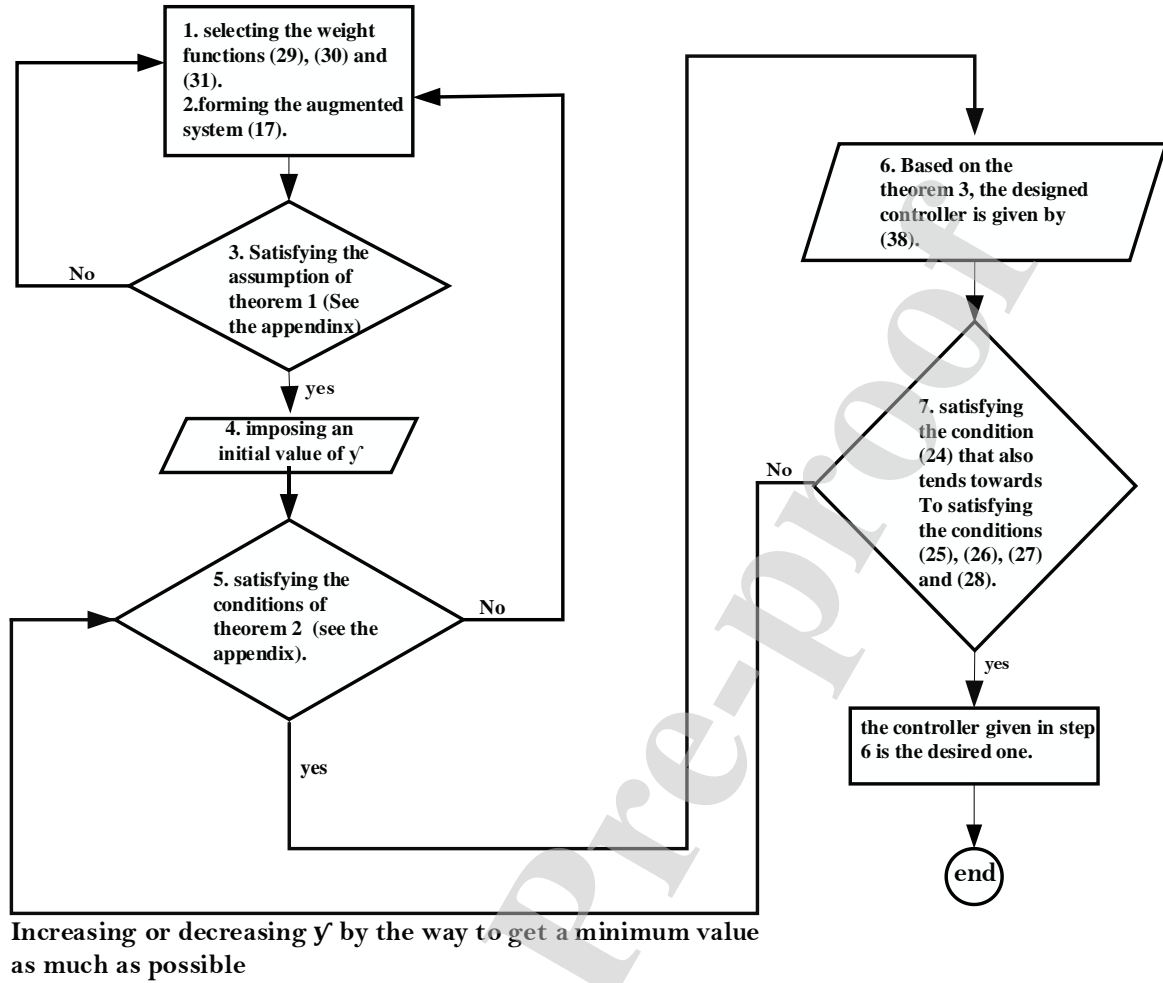


Fig. 15. GDOA flowchart.

The derived controller described in (38) can ensure the stability of the studied system under the presence of CPLs and avoiding the effect of the whole perturbations. To validate the effectiveness of the derived controller, the stability analysis and both simulation and experimental setup are carried out and presented in the next sections.

6. Stability analysis

The stability analysis of the studied system under applying the derived controller requires the verification of the conditions (25-28). Using the bode plot, the sensitivity and weight functions have been analyzed, as illustrated in Fig. 16. The system parameters are listed in Table 1.

Table 1. System parameters.

Variables	Descriptions	values
V_{ref}	Reference Bus Voltage	140 V
V_{in}	DC Power Supply Voltage	280 V
C_0	Capacitance Nominal Value	220 μ F
L_0	Inductance Nominal Value	2.7 mH
r_L	Parasite Inductance Resistance	0.8 Ω
f_s	Switching Frequency	25 kHz

According to the developed algorithm, the selected weight functions and the resulting robust controller are given by:

$$\begin{cases} W_1(s) = \frac{0.75 \cdot s + 8 \cdot 10^3}{s + 0.8} \\ W_2(s) = \frac{s \cdot 10^3 + 6 \cdot 10^7}{s + 6 \cdot 10^7} \\ W_3(s) = 5 \cdot 10^5 \end{cases} \quad (39)$$

and,

$$K_\infty(s) = \frac{733.6s^3 + 5.869 \cdot 10^3 s^2 + 7.011 \cdot 10^3 s + 4.987 \cdot 10^{16}}{s^4 + 4.351 \cdot 10^6 s^3 + 1.696 \cdot 10^{11} s^2 + 3.188 \cdot 10^5 s + 2.55 \cdot 10^5} \quad (40)$$

where,

$$\gamma = 1.28 \quad (41)$$

According to the voltage closed-loop control system (see Fig. 11) and without considering the weight functions, the control u and y error variables are given by:

$$\begin{bmatrix} y \\ u \end{bmatrix} = \overbrace{\begin{bmatrix} S(s) & S(s)T_{p_0}(s) \\ S(s)K_\infty(s) & T(s) \end{bmatrix}}^{H(s)} \cdot \begin{bmatrix} V_{ref} \\ \varpi \end{bmatrix} \quad (42)$$

Fig. 16 shows that the conditions (25-28) are satisfied. Moreover, the amplitudes of the elements $H(s)$ are lower than 1. That means the derived controller can mitigate the negative effect of the perturbations and to keep the control variable u depending only on the error variable y , as it is expressed in (18).

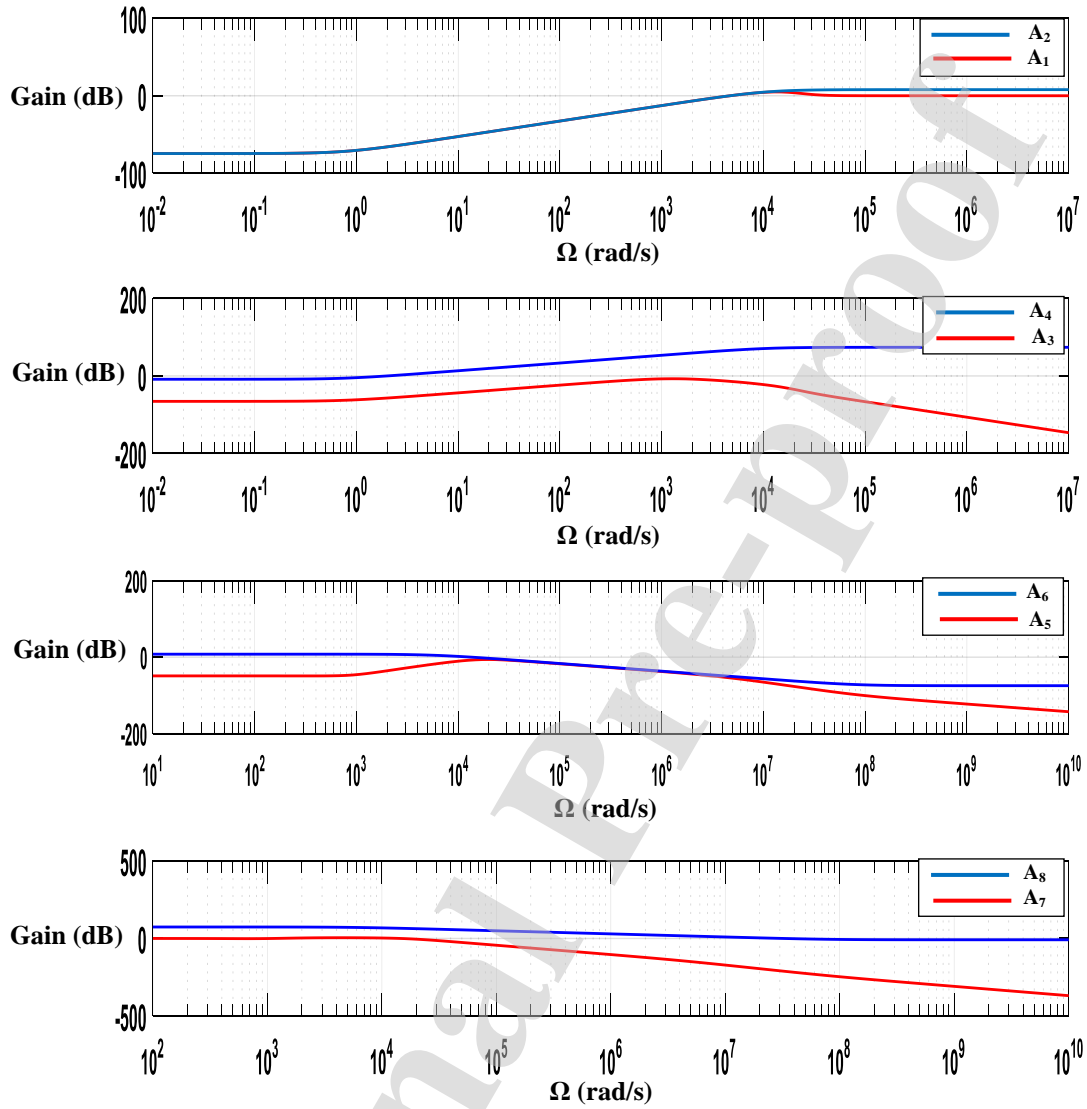


Fig. 16. Frequency analysis of the conditions (25-28)

Fig. 17 depicts the poles evolution in the discrete-time of the studied system before and after applying the derived controller, where: the poles that are denoted by the red color present the system dynamic before applying the robust control and the poles that are denoted by the blue color present the system dynamic after applying the robust control. The derived controller guarantees stability performance during the system operation.

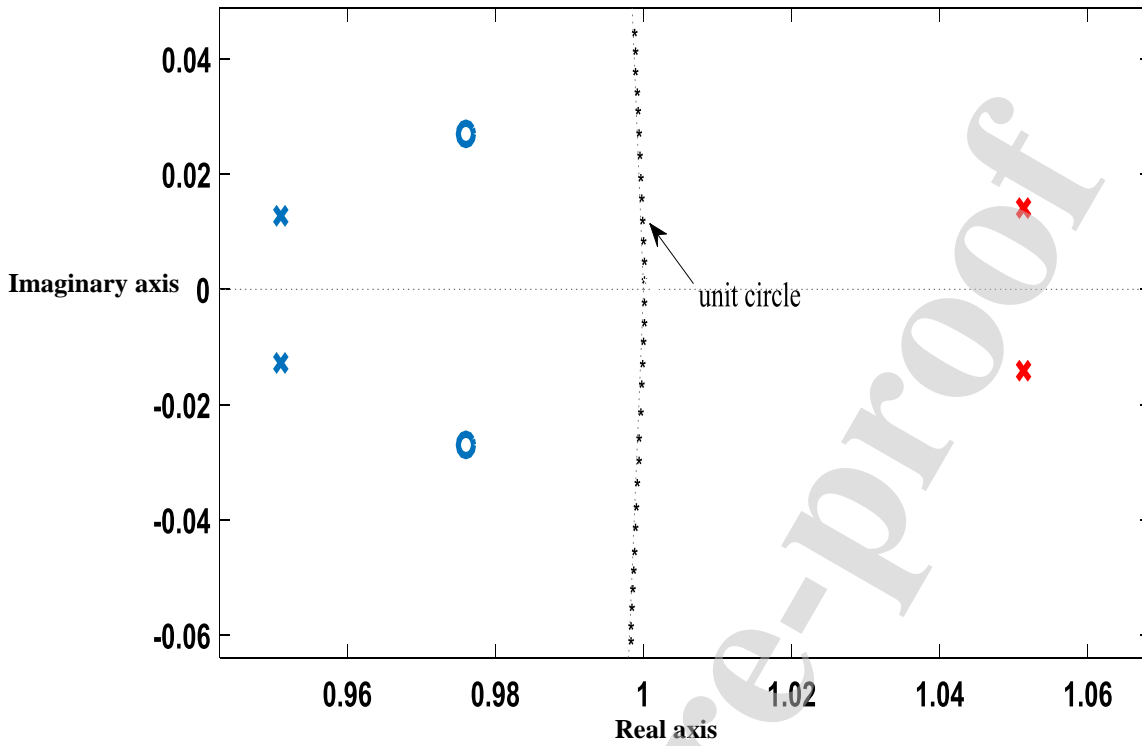


Fig. 17. Pole-zero plot of the studied system before and after applying the robust controller.

For exhibiting the enhancement that will be shown in the output voltage and load current behaviors brought by the obtained controller, simulation study is carried out and will be presented in the following section.

7. Simulation results

To validate the effectiveness of the derived controller, the studied system in the presence of CPL illustrated in Fig. 18 is simulated in PSIM software. The system parameters taken in this simulation are the same given in Table 1. The CPL is modeled as a current controlled source, thus enabling to adjust the power consumed by the CPL. The simulation study is subdivided into three scenarios. The first scenario is a simulation of sudden changes of the demanded power by the CPL to assess the controller's robustness against current fluctuation. The second scenario is the assessment against input voltage fluctuations. The last scenario is carried out to verify the robustness of the derived controller against parameter variations. The simulation results are shown in Fig. 19, Fig. 20 and Fig. 21.

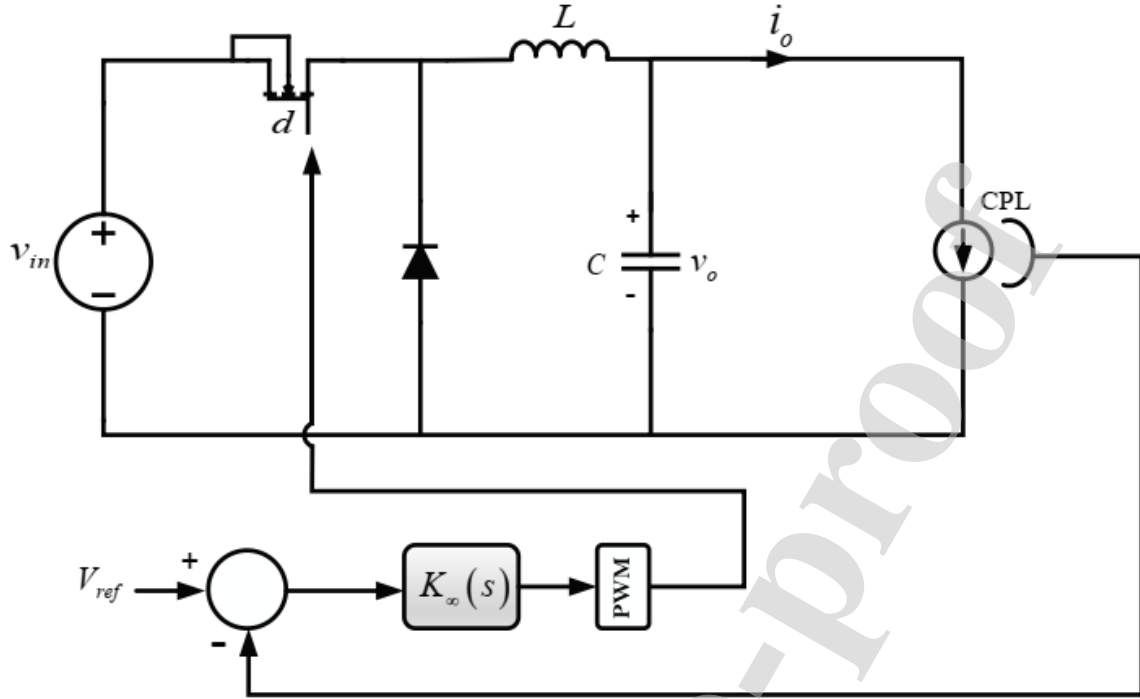


Fig. 18. buck converter feeding CPL unit operating under robust control.

According to Fig. 19 and Fig. 20, the studied system operation under the derived control has a transient dynamic that corresponds to a settling time less than 0.04 s and the output voltage remains at the voltage reference in the steady-state with a small error. The sudden changes in the power consumed by the CPL cause the small transient voltage deviations. After that, the output voltage is kept at the voltage reference. The disturbance brought by the CPL current is well contained and has no instability risks.

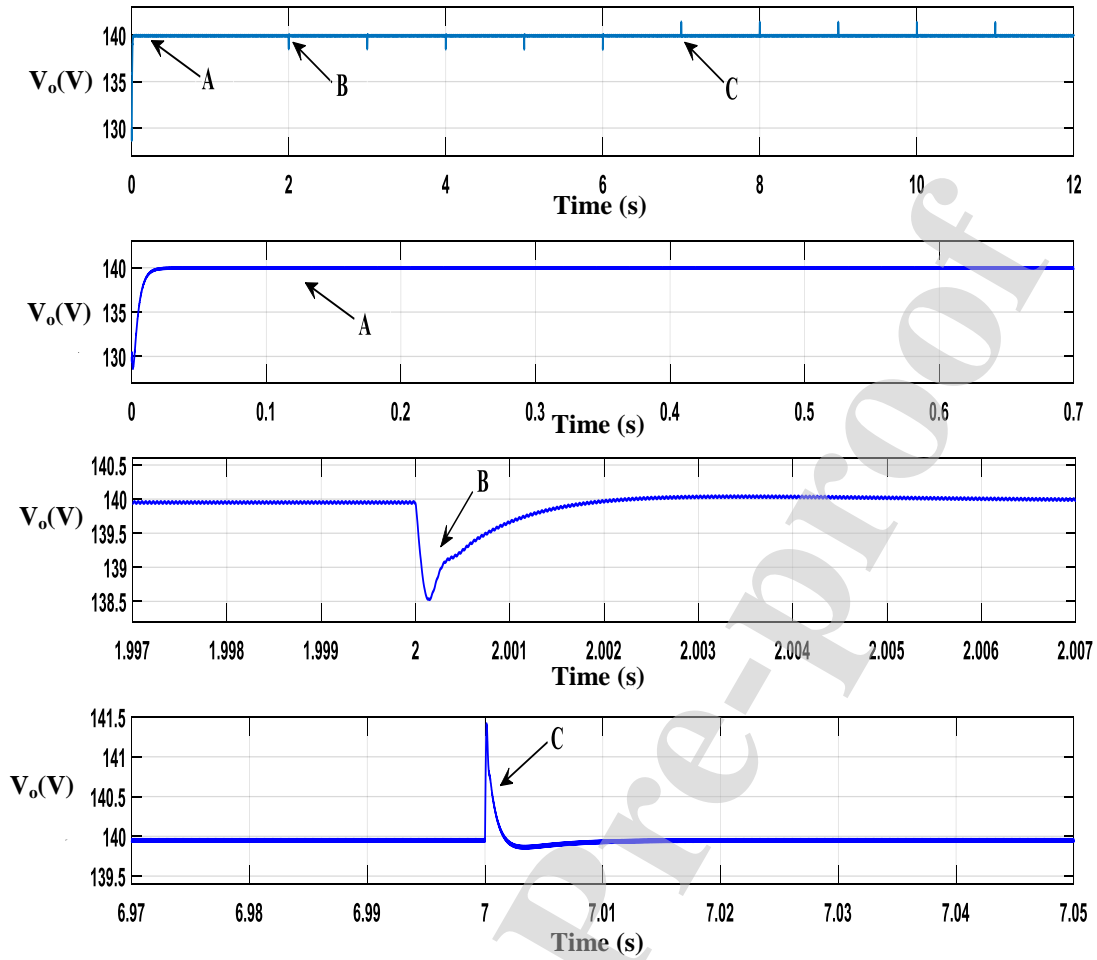


Fig. 19. Output voltage behavior under the simulation scenario of the different step changes of the power consumed by the CPL.

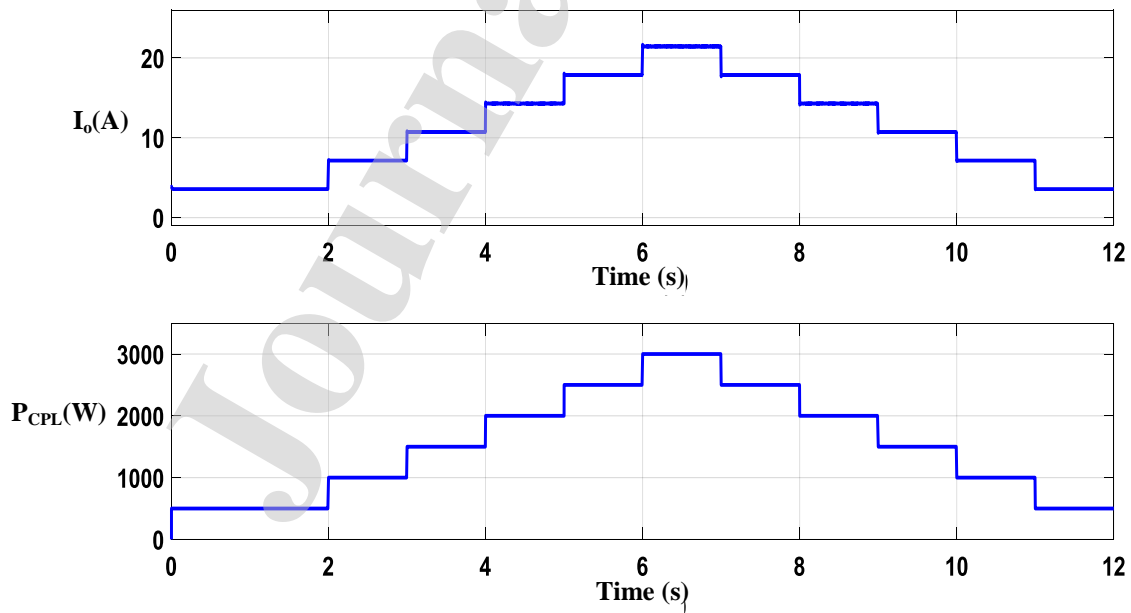


Fig. 20. CPL's current behavior under the simulation scenario of the different step-changes of the power consumed by the CPL.

The effect of a sudden change in the input voltage on the output voltage is shown in Fig. 21. Although, the transition of the input voltage is significant ($\pm 15\text{V}$), the effect on the output voltage is almost negligible. The output voltage undergoes a small change for a short time and returns to the reference voltage.

The parameter variations test is carried out as follows; From 3.33s to 6.66s, the capacitance and inductance values are decreased by -30% and -60% respectively. From 6.66s to 10s, the capacitance is increased by 120% and the inductance is kept at the nominal value. Noticing that, at the instants 3.33 s and 6.66s, a sudden transit voltage deviation is occurred, which is caused by the sudden changes of the inductance and capacitance. However, for the rest of the time, the output voltage is kept at the desired voltage with a small steady-state error as it is shown in Fig. 22.

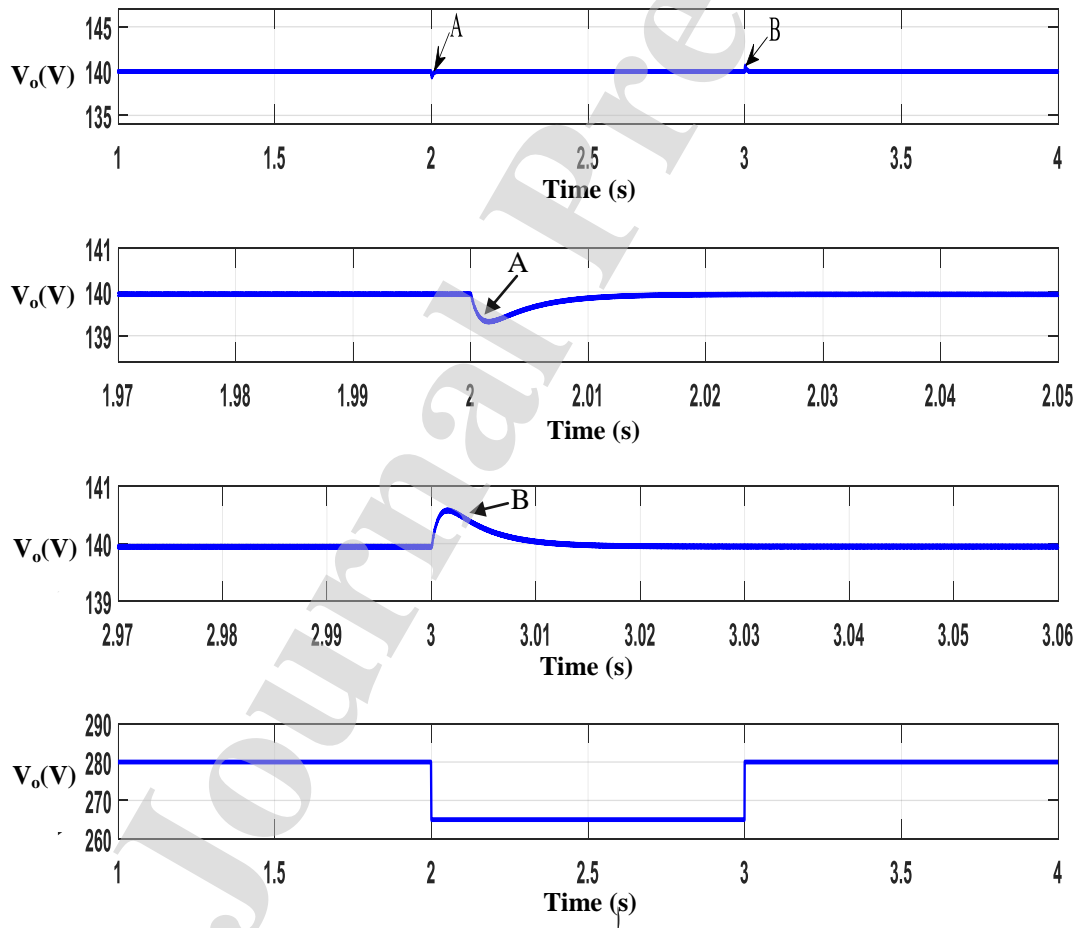


Fig. 21. Output voltage behavior under the input voltage variation test scenario.

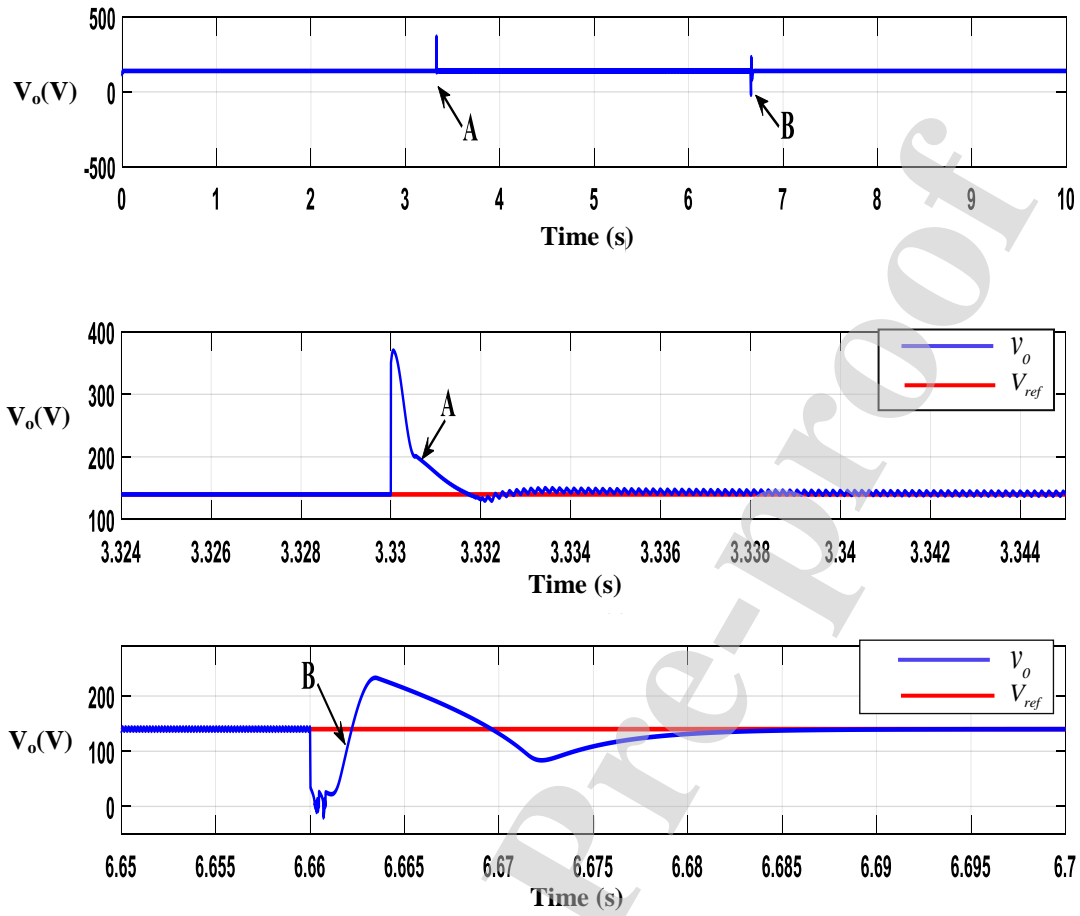


Fig. 22. Output voltage behavior under parameter variation test scenario.

7. Experimental results

The experimental setup shown in Fig. 23 is built in the laboratory to validate the effectiveness of the derived controller, which consists of a DC source, DC/DC buck converter and a boost converter acting as a CPL. The load side converter (boost converter), whose output voltage is firmly regulated, feeds a resistive load. The power demand of the CPL is adjusted by changing the resistance load. Two experimental tests are carried out: the first is a variation test of CPL power demand (CPL power is adjusted by the resistance of boost converter) and the second test is an input voltage variation. The desired output voltage is 15 V and the DC source voltage is 28 V. The experimental results are depicted in Fig. 24, Fig. 25 and Fig. 26.

It is worth mentioning here that the capacitance and inductance values used in the experimental setup are different from those listed in Table 1. While the controller is designed using the parameters listed in Table 1 in order to validate its robustness against the parameter

variations. The adopted parameters for the experiment purpose are listed in Table 2. The designed controller is implemented in a low cost DSP of Texas Instrument TMS320F28335. Using the controller order reduction algorithm [62], the designed controller converted to a discrete-time is given as follows:

$$K_{\infty}(Z) = \frac{4.47Z^2 - 4.37 \cdot Z + 4.379}{Z^3 - 1.177Z^2 + 0.186Z - 0.009} \quad (43)$$

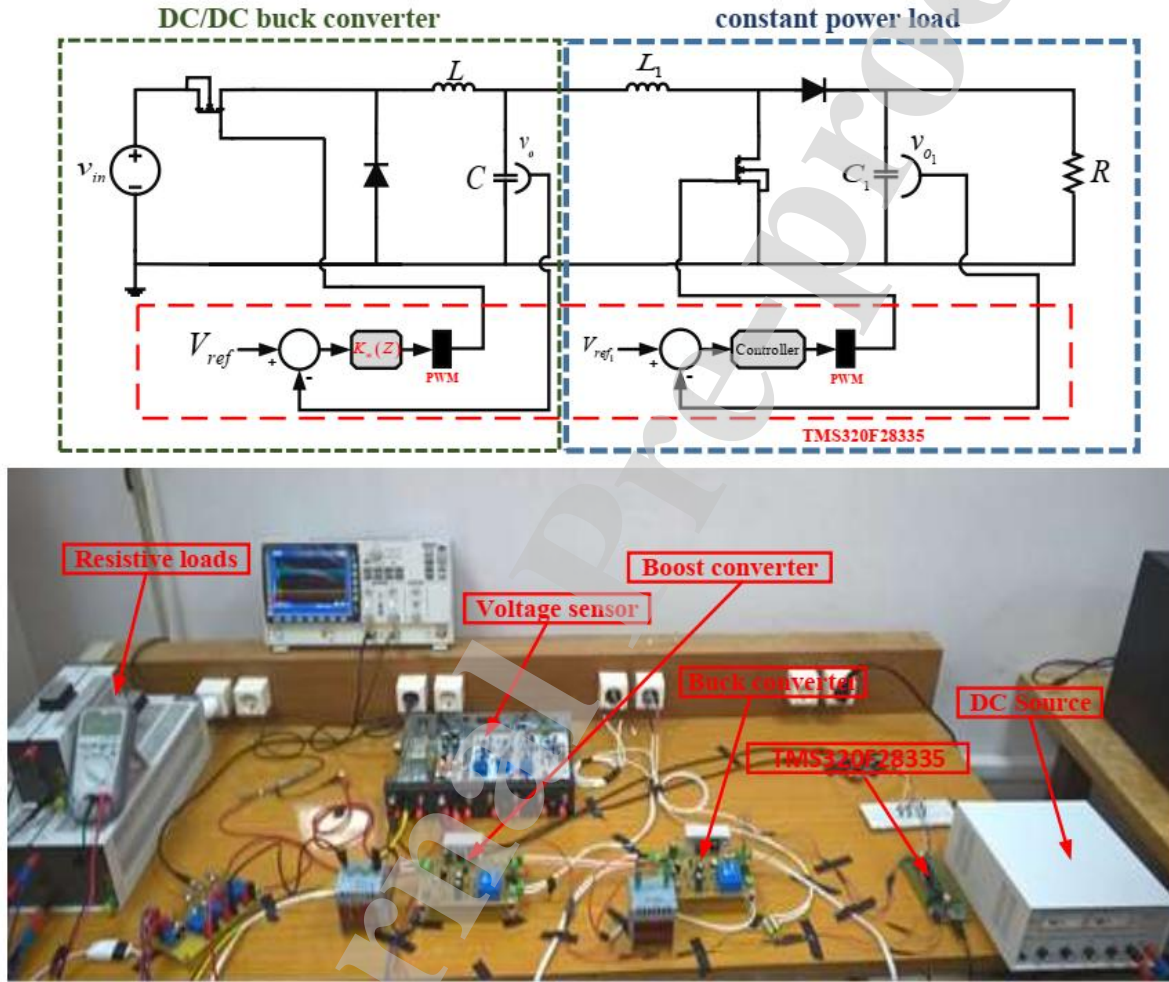
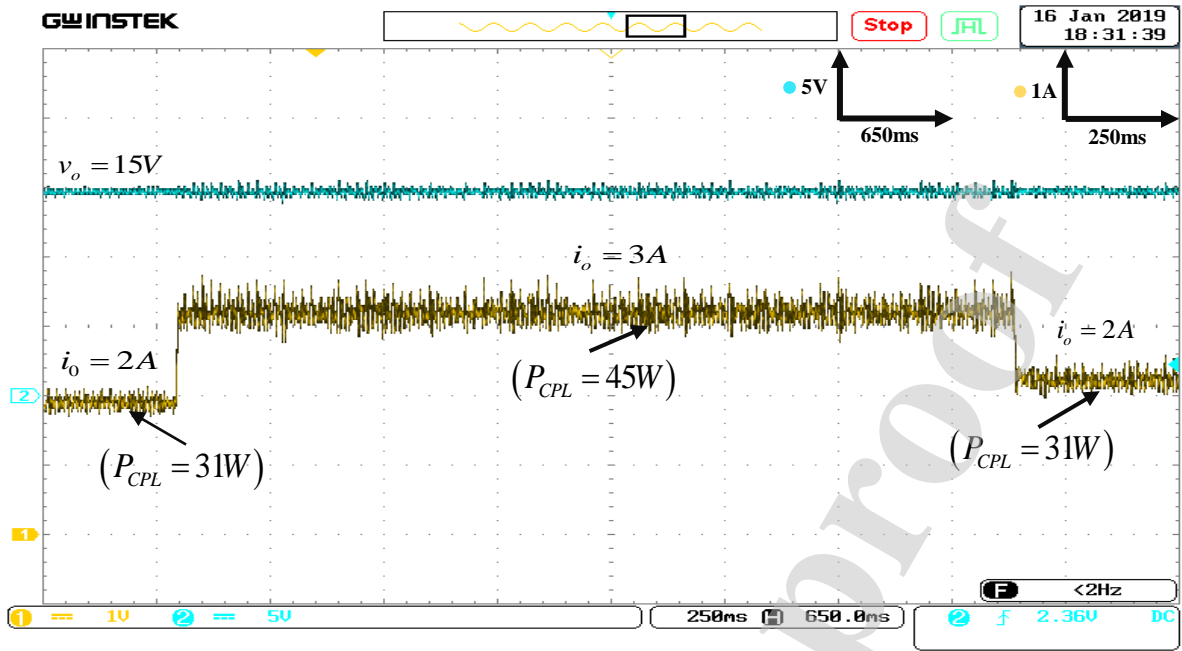
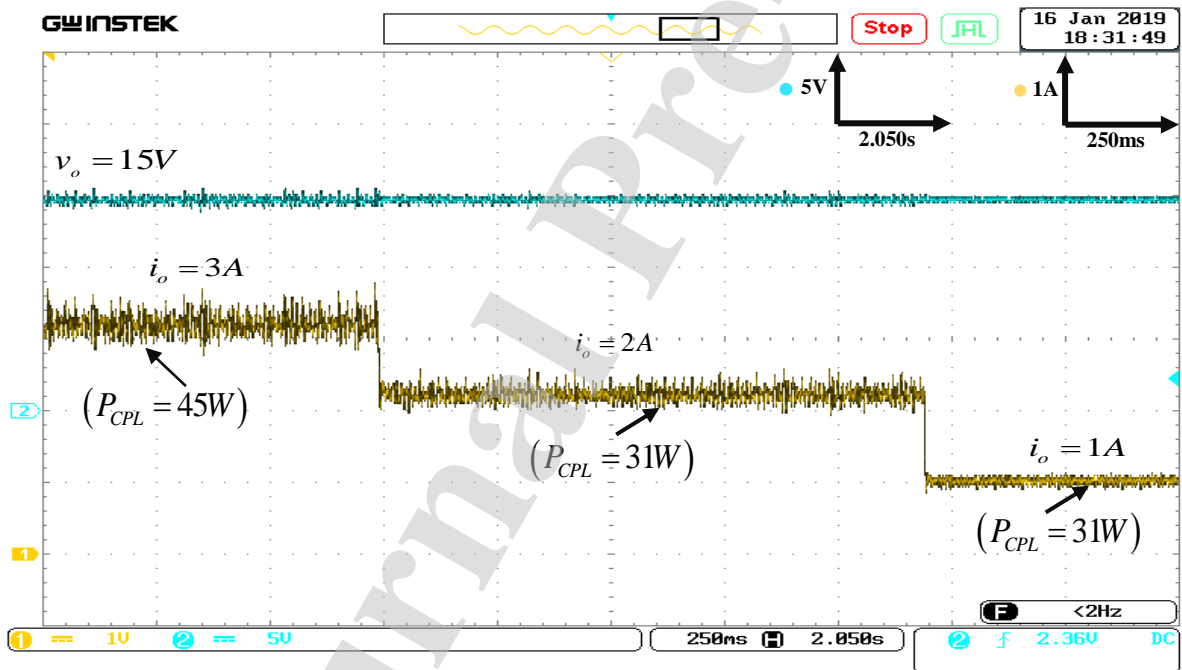


Fig. 23. Experimental setup.



455



456

457

Fig. 24. Experimental results of CPL consumed power variation test.

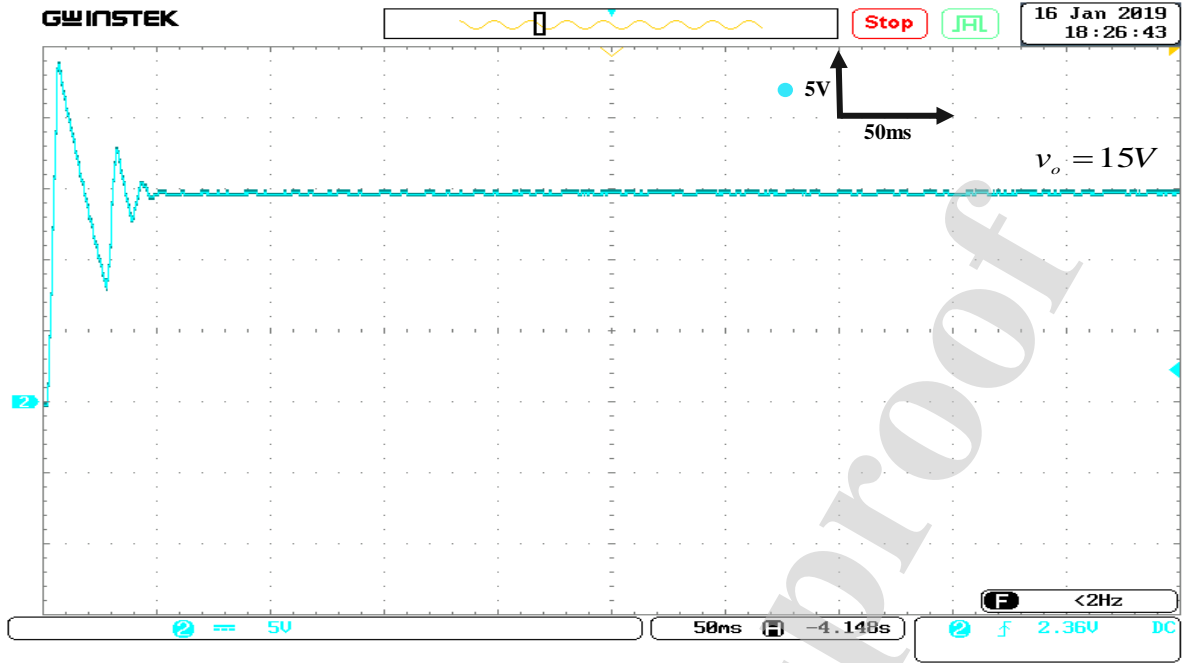


Fig. 25. Transit dynamic of output voltage response.

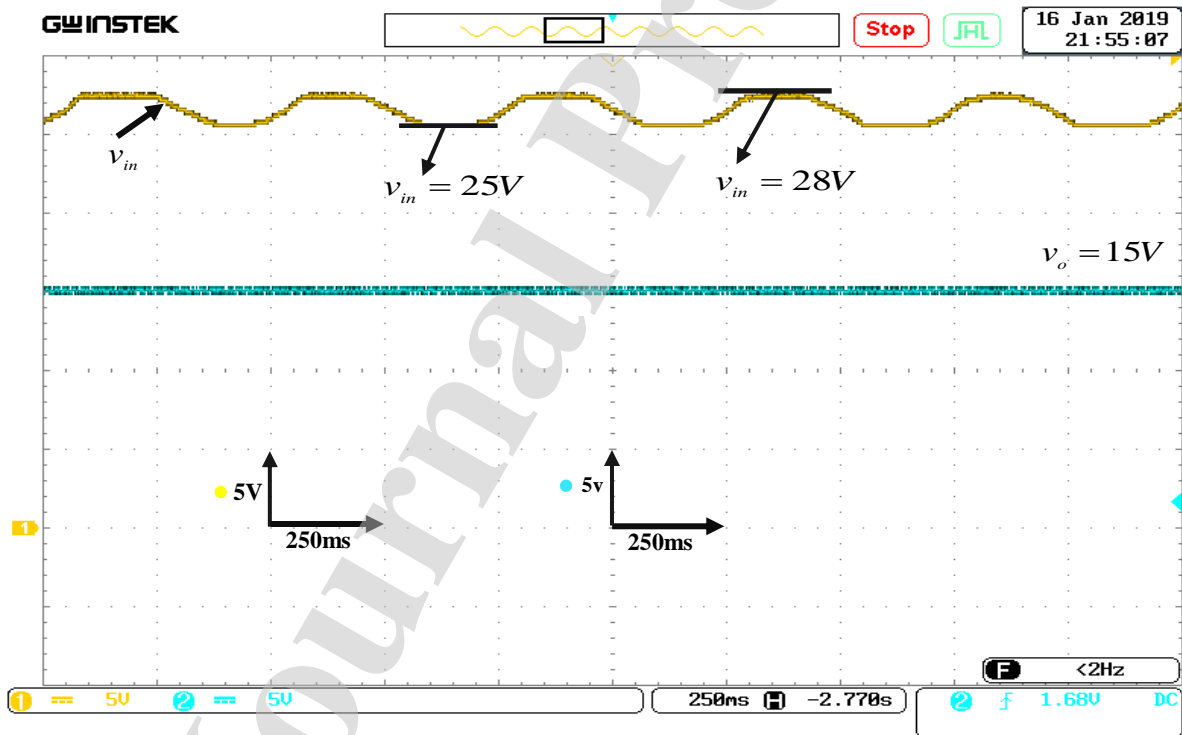


Fig. 26. Experimental results of input voltage variation test.

According to Fig. 24, Fig. 25 and Fig. 26, the system operation has a short transient dynamic, which corresponds to a small settling time less than 0.04 s. The output voltage has an allowed overshoot and remains at the desired value. Moreover, the system stability is maintained

under several changes of the power consumed by the CPL. The controller is robust against the parameter variations and avoids the perturbations brought by the CPL current and input voltage fluctuations. Any transient voltage deviation appears when a substantial change occurred in the input voltage and power consumed by CPL.

Table 2. Experimental setup parameters.

Variables	Buck converter	Boost converter
Voltage Reference	$V_{ref} = 15V$	$V_{ref_1} = 20V$
Input Voltage	$V_{in} = 28V$	$v_o = 15V$
Capacitance	$C = 470\mu F$	$C_1 = 470\mu F$
Inductance	$L = 2.87mH$	$L_1 = 0.5mH$
Switching Frequency	$25kHz$	$25kHz$
R	///	$9\Omega(45W)$
	///	$13\Omega(31W)$
	///	$25\Omega(15W)$

8. Conclusion

In this paper, the instability issues caused by the presence of constant power loads in a DC microgrid have been addressed. A H_∞ -based controller has been designed to ensure stable operation of the DC-MG when supplying CPLs. In addition the designed controller is able to reject all possible perturbations such as those attributed to parameters variation and input voltage fluctuations. The design process of the proposed controller was based on GDOA and weight functions to obtain a robust control and reaching the desired performances. The effectiveness of the proposed method has been assessed by simulation and experimentally validated by using low cost DSP board.

In some cases, GDOA provides a robust controller having a higher order of the denominator, which is difficult to implement. So, to make the implementation easier, reducing the denominator order of the controller calls the use of a specific algorithm that may lead to losing control performances. Future work consists of proposing another design process of H_∞ norm and specific optimization algorithm, which allows fixing the structure of the desired control to cover the disadvantage mentioned before. This algorithm does not require the use of reduction algorithms and can provide the structured H_∞ based controller that can have a lower order of denominator and achieves the desired performances and guarantees the system stability.

489

490 **Acknowledgments**

491 This work was supported in part by the Direction Generale de la Recherche Scientifique et du
 492 Développement Technologique, DGRSDT, of Algeria.

493 **References.**

494 [1] S. Rezaee, S. Ebrahimi, N. Amiri, Y. Huang, and J. Jatskevich, "Accurate and fast
 495 power-sharing among inverters in AC microgrids with constant power loads," 2017 IEEE
 496 18th Workshop on Control and Modeling for Power Electronics (COMPEL), Jul. 2017.

497 [2] Zhang, Zhuang, Liu, Wang, and Guo, "A Novel Autonomous Current-Sharing Control
 498 Strategy for Multiple Paralleled DC-DC Converters in Islanded DC Microgrid," *Energies*, vol.
 499 12, no. 20, p. 3951, Oct. 2019.

500 [3] . M. Guerrero, J. C. Vasquez, and R. Teodorescu, "Hierarchical control of droop-
 501 controlled DC and AC microgrids — a general approach towards standardization," 2009 35th
 502 Annual Conference of IEEE Industrial Electronics, Nov. 2009.

503 [4] Y. Han, X. Ning, P. Yang, and L. Xu, "Review of Power Sharing, Voltage Restoration
 504 and Stabilization Techniques in Hierarchical Controlled DC Microgrids," *IEEE Access*, vol.
 505 7, pp. 149202–149223, 2019.

506 [5] M. Castilla, A. Camacho, P. Marti, M. Velasco, and M. M. Ghahderijani, "Impact of
 507 Clock Drifts on Communication-Free Secondary Control Schemes for Inverter-Based
 508 Islanded Microgrids," *IEEE Transactions on Industrial Electronics*, vol. 65, no. 6, pp. 4739–
 509 4749, Jun. 2018.

510 [6] A. Khatibzadeh, M. Besmi, A. Mahabadi, and M. Reza Haghifam, "Multi-Agent-
 511 Based Controller for Voltage Enhancement in AC/DC Hybrid Microgrid Using Energy
 512 Storages," *Energies*, vol. 10, no. 2, p. 169, Feb. 2017.

513 [7] J. Baek, W. Choi, and S. Chae, "Distributed Control Strategy for Autonomous
 514 Operation of Hybrid AC/DC Microgrid," *Energies*, vol. 10, no. 3, p. 373, Mar. 2017.

515 [8] J. Baek, W. Choi, and S. Chae, "Distributed Control Strategy for Autonomous
 516 Operation of Hybrid AC/DC Microgrid," *Energies*, vol. 10, no. 3, p. 373, Mar. 2017.

- [9] R. Salas-Puente, S. Marzal, R. González-Medina, E. Figueres, and G. Garcera, "Experimental Study of a Centralized Control Strategy of a DC Microgrid Working in Grid-Connected Mode," *Energies*, vol. 10, no. 10, p. 1627, Oct. 2017.
- [10] W. Issa, Al-naemi Faris, G. Konstantopoulos, S. Sharkh, and M. Abusara, "Stability Analysis and Control of a Microgrid against Circulating Power between Parallel Inverters," *Energy Procedia*, vol. 157, pp. 1061–1070, Jan. 2019.
- [11] S. Yousefizadeh, J. D. Bendtsen, N. Vafamand, M. H. Khooban, T. Dragicevic, and F. Blaabjerg, "EKF-Based Predictive Stabilization of Shipboard DC Microgrids With Uncertain Time-Varying Load," *IEEE Journal of Emerging and Selected Topics in Power Electronics*, vol. 7, no. 2, pp. 901–909, Jun. 2019.
- [12] S. Pang, B. Nahid-Mobarakeh, S. Pierfederici, Y. Huangfu, G. Luo, and F. Gao, "Research on LC Filter Cascaded with Buck Converter Supplying Constant Power Load Based on IDA-Passivity-Based Control," *IECON 2018 - 44th Annual Conference of the IEEE Industrial Electronics Society*, Oct. 2018.
- [13] N. Zhao, G. Wang, D. Ding, G. Zhang, and D. Xu, "Impedance Based Stabilization Control Method for Reduced DC-Link Capacitance IPMSM Drives," *IEEE Transactions on Power Electronics*, vol. 34, no. 10, pp. 9879–9890, Oct. 2019.
- [14] M. N. Hussain and V. Agarwal, "A Novel Feedforward Stabilizing Technique to Damp Power Oscillations Caused by DC-DC Converters fed from a DC bus," *IEEE Journal of Emerging and Selected Topics in Power Electronics*, pp. 1–1, 2019.
- [15] K. E. L. Marcillo, D. A. P. Guingla, W. Barra, R. L. P. De Medeiros, E. M. Rocha, D. A. V. Benavides, and F. G. Nogueira, "Interval Robust Controller to Minimize Oscillations Effects Caused by Constant Power Load in a DC Multi-Converter Buck-Buck System," *IEEE Access*, vol. 7, pp. 26324–26342, 2019.
- [16] J. Wu and Y. Lu, "Adaptive Backstepping Sliding Mode Control for Boost Converter With Constant Power Load," *IEEE Access*, vol. 7, pp. 50797–50807, 2019.
- [17] H. Saberi, S. Mehraeen, and M. M. Rezvani, "Intelligent Operation of Small-Scale Interconnected DC Grids via Measurement Redundancy," *IEEE Transactions on Industrial Electronics*, vol. 66, no. 11, pp. 9086–9096, Nov. 2019.

- [18] K. Potty, E. Bauer, C. Moya, B. Sim, and J. Wang, "Smart Resistor for Stability Improvement of the dc Link in Turbo-Electric Aircrafts," 2019 IEEE Applied Power Electronics Conference and Exposition (APEC), Mar. 2019.
- [19] C. Zhang, X. Wang, P. Lin, P. X. Liu, Y. Yan, and J. Yang, "Finite-Time Feedforward Decoupling and Precise Decentralized Control for DC Microgrids Towards Large-Signal Stability," IEEE Transactions on Smart Grid, pp. 1–1, 2019.
- [20] A. Marcos-Pastor, E. Vidal-Idiarte, A. Cid-Pastor, and L. Martinez-Salamero, "Minimum DC-link Capacitance for Single-Phase Applications with Power Factor Correction," IEEE Transactions on Industrial Electronics, pp. 1–1, 2019.
- [21] Mustafa. Alrayah.Hassan, Er-Ping.Li, Xue.Li, Tianhang.Li, Chenyang.Duan and Song.Chi, "Adaptive Passivity-Based Control of DC-DC Buck Converter With Constant Power Load in DC Microgrid Systems", IEEE JOURNAL OF EMERGING AND SELECTED TOPICS IN POWER ELECTRONICS,2018.
- [22] S. Sumsurooah, M. Odavic, and S. Bozhko, "μ Approach to Robust Stability Domains in the Space of Parametric Uncertainties for a Power System With Ideal CPL," IEEE Transactions on Power Electronics, vol. 33, no. 1, pp. 833–844, Jan. 2018.
- [23] Mohammed KH.AL-Nussairi, Ramza.Bayindir, Samjeevikumar.Padmanaban, Lucian.Mihet-Popa and Pierluigi.Siano, "Constant Power Load (CPL) with Microgrids: Problem Definition, Stability Analysis, and Compensation Techniques",pp.1-20, energies 2017.
- [24] Mauricio.Céspedes, Troy.beechner, Lei.King and Jian.Sun, "Stabilization of Constant-Power Loads By Passive Impedance Damping".2010 Twenty-Fifth Annual IEEE Applied Power Electronics Conference and Exposition (APEC),pp.2174-2180, March 2010
- [25] Xinbo.Liu, Yawei.Bian and Shengwen.Fan, "Active Stabilization Control for Storage System Paralleled with Constant Power Loads",20th International Conference on Electrical Machines and Systems (ICEMS),2017.
- [26] Xinbo.Liu and Shuohan.Ma," Large Signal Stabilization Method of Constant Lower Loads by Adding R Parallel Dampings Filters". IEEE Energy Conversion Congress and Exposition (ECCE), pp.1314-1319, step 2015.

- [27] A.Khaligh, "Realization of Parasitics in Stability of DC-DC Converters Loaded by Constant Power Loads in Advanced Multiconverter Automotive Systems," IEEE Transactions on Industrial Electronics, vol. 55, no. 6, pp. 2295–2305, Jun. 2008.
- [28] A.Khaligh, P.Chapman, A.Davoudi, and J.Jatskevich, "Realization of Parasitics in the Stability of Dc-Dc Converters Loaded by Constant-Power Loads in Discontinuous Conduction Mode," 2007 IEEE Vehicle Power and Propulsion Conference, Sep. 2007.
- [29] Yiming Tu, Zeng Liu, Jinjun Liu, Teng Liu, and Zipeng Liu, "An additional stabilizer for mitigating the instability in DC/DC cascaded system with constant power loads," 2017 IEEE 3rd International Future Energy Electronics Conference and ECCE Asia (IFEEC 2017 - ECCE Asia), Jun. 2017.
- [30] Xiaonan.Lu, Kai.Sun, Lipei.Huang, Josep M.Guerrero, Jane.C, and Yan.Xing, "Virtual Impedance Based Stability Improvement for DC Microgrid with Constant Power Loads", IEEE Energy Conversion Congress and Exposition (ECCE). pp.2670-2675, sept.2014.
- [31] W. Cai, B. Fahimi, E. Cosoroaba, and F. Yi, "Stability analysis and voltage control method based on virtual resistor and proportional voltage feedback loop for cascaded DC-DC converters," 2014 IEEE Energy Conversion Congress and Exposition (ECCE), Sep. 2014.
- [32] D.M.Vilathgamuwa, X.N.Zhang, S.D.G.Jayasinghe, B.S.Bhangu, C.J.Gajanayake, King Jet Tseng," Virtual Resistance Based Active Damping Solution for Constant Power Load Instability in AC Microgrid", IECON 2011 - 37th Annual Conference of the IEEE Industrial Electronics Society, PP.3646-3651, November 2011.
- [33] H. Abdollahi, S. Arrua, T. Roinila, and E. Santi, "A Novel DC Power Distribution System Stabilization Method Based on Adaptive Resonance-Enhanced Voltage Controller," IEEE Transactions on Industrial Electronics, vol. 66, no. 7, pp. 5653–5662, Jul. 2019.
- [34] M. N. Hussain and V. Agarwal, "A Novel Feedforward Stabilizing Technique to Damp Power Oscillations Caused by DC-DC Converters fed from a DC bus," IEEE Journal of Emerging and Selected Topics in Power Electronics, pp. 1–1, 2019.
- [35] S. Liu, P. Su, and L. Zhang, "A Nonlinear Disturbance Observer-Based Virtual Negative Inductor Stabilizing Strategy for DC Microgrid with Constant Power Loads," Energies, vol. 11, no. 11, p. 3174, Nov. 2018.

- [36] Q. Xu, C. Zhang, C. Wen, and P. Wang, "A Novel Composite Nonlinear Controller for Stabilization of Constant Power Load in DC Microgrid," *IEEE Transactions on Smart Grid*, vol. 10, no. 1, pp. 752–761, Jan. 2019.
- [37] T. Dragicevic, "Dynamic Stabilization of DC Microgrids with Predictive Control of Point-of-Load Converters," *IEEE Transactions on Power Electronics*, vol. 33, no. 12, pp. 10872–10884, Dec. 2018.
- [38] N. Vafamand, M. H. Khooban, T. Dragicevic, and F. Blaabjerg, "Networked Fuzzy Predictive Control of Power Buffers for Dynamic Stabilization of DC Microgrids," *IEEE Transactions on Industrial Electronics*, vol. 66, no. 2, pp. 1356–1362, Feb. 2019.
- [39] S. Yousefizadeh, J. D. Bendtsen, N. Vafamand, M. H. Khooban, T. Dragicevic, and F. Blaabjerg, "EKF-Based Predictive Stabilization of Shipboard DC Microgrids With Uncertain Time-Varying Load," *IEEE Journal of Emerging and Selected Topics in Power Electronics*, vol. 7, no. 2, pp. 901–909, Jun. 2019.
- [40] N. Vafamand, S. Yousefizadeh, M. H. Khooban, J. D. Bendtsen, and T. Dragicevic, "Adaptive TS Fuzzy-Based MPC for DC Microgrids With Dynamic CPLs: Nonlinear Power Observer Approach," *IEEE Systems Journal*, vol. 13, no. 3, pp. 3203–3210, Sep. 2019.
- [41] S. Yousefizadeh, J. D. Bendtsen, N. Vafamand, M. H. Khooban, T. Dragicevic, and F. Blaabjerg, "EKF-Based Predictive Stabilization of Shipboard DC Microgrids With Uncertain Time-Varying Load," *IEEE Journal of Emerging and Selected Topics in Power Electronics*, vol. 7, no. 2, pp. 901–909, Jun. 2019.
- [42] R. Cheng, J. F. Forbes, and W. S. Yip, "Price-driven coordination method for solving plant-wide MPC problems," *Journal of Process Control*, vol. 17, no. 5, pp. 429–438, Jun. 2007.
- [43] Yue Zhao, Wei Qiao, and Daiyun Ha, "A Sliding-Mode Duty-Ration Controller for DC/DC Buck Converters With Constant Power Loads," *IEEE TRANSACTIONS ON INDUSTRY APPLICATIONS*, VOL. 50, NO. 2, pp.1448-1458 ,MARCH/APRIL 2014.
- [44] E. Hossain, R. Perez, S. Padmanaban, L. Mihet-Popa, F. Blaabjerg, and V. Ramachandaramurthy, "Sliding Mode Controller and Lyapunov Redesign Controller to

- 633 Improve Microgrid Stability: A Comparative Analysis with CPL Power Variation,” *Energies*,
 634 vol. 10, no. 12, p. 1959, Nov. 2017.
- 635 [45] E.-C. Chang, “Study and Application of Intelligent Sliding Mode Control for Voltage
 636 Source Inverters,” *Energies*, vol. 11, no. 10, p. 2544, Sep. 2018.
- 637 [46] A. Yasin, M. Ashraf, and A. Bhatti, “Fixed Frequency Sliding Mode Control of Power
 638 Converters for Improved Dynamic Response in DC Micro-Grids,” *Energies*, vol. 11, no. 10,
 639 p. 2799, Oct. 2018.
- 640 [47] A. El Aroudi, B. Martínez-Treviño, E. Vidal-Idiarte, and A. Cid-Pastor, “Fixed
 641 Switching Frequency Digital Sliding-Mode Control of DC-DC Power Supplies Loaded by
 642 Constant Power Loads with Inrush Current Limitation Capability,” *Energies*, vol. 12, no. 6, p.
 643 1055, Mar. 2019.
- 644 [48] J. L. Anderson Azzano, J. J. Moré, and P. F. Puleston, “Stability Criteria for Input
 645 Filter Design in Converters with CPL: Applications in Sliding Mode Controlled Power
 646 Systems,” *Energies*, vol. 12, no. 21, p. 4048, Oct. 2019.
- 647 [49] A. M. Rahimi and A. Emadi, “Active Damping in DC/DC Power Electronic
 648 Converters: A Novel Method to Overcome the Problems of Constant Power Loads,” *IEEE*
 649 *Transactions on Industrial Electronics*, vol. 56, DOI: 10.1109/TIE.2009.2013748, no. 5, pp.
 650 1428–1439, May 2009.
- 651 [50] S. Yousefizadeh, J. D. Bendtsen, N. Vafamand, M. H. Khooban, F. Blaabjerg, and T.
 652 Dragicevic, “Tracking Control for a DC Microgrid Feeding Uncertain Loads in More Electric
 653 Aircraft: Adaptive Backstepping Approach,” *IEEE Transactions on Industrial Electronics*,
 654 vol. 66, no. 7, pp. 5644–5652, Jul. 2019.
- 655 [51] S. Pang, B. Nahid-Mobarakeh, S. Pierfederici, M. Phattanasak, Y. Huangfu, G. Luo,
 656 and F. Gao, “Interconnection and Damping Assignment Passivity-Based Control Applied to
 657 On-Board DC–DC Power Converter System Supplying Constant Power Load,” *IEEE*
 658 *Transactions on Industry Applications*, vol. 55, no. 6, pp. 6476–6485, Nov. 2019.
- 659 [52] S. Pang, B. Nahid-Mobarakeh, S. Pierfederici, Y. Huangfu, G. Luo, and F. Gao,
 660 “Towards Stabilization of Constant Power Loads Using IDA-PBC for Cascaded LC filter
 661 DC/DC Converters,” *IEEE Journal of Emerging and Selected Topics in Power Electronics*,
 662 pp. 1–1, 2019.

- [53] X. Lu, K. Sun, L. Huang, J. M. Guerrero, J. C. Vasquez, and Y. Xing, "Virtual impedance based stability improvement for DC microgrids with constant power loads," 2014 IEEE Energy Conversion Congress and Exposition (ECCE), Sep. 2014.
- [54] Jang Lee Hong, Ching-Cheng Teng," A Derivation of the Golver-Doyle Algorithms for General H^∞ Control Problems", Automatica, Vol.32, No.4, pp.581-589,1996.
- [55] Amin S.Meghani and Haniph A.Latchman," H_∞ Vs.Classical Methods in the Design of Feedback Control Systems" ,Proceedings IEEE Southeastcon '92,pp.59-62, April 1992.
- [56] M. Makarov, M. Grossard, P. Rodriguez-Ayerbe, and D. Dumur, "Modeling and Preview H_∞ Control Design for Motion Control of Elastic-Joint Robots With Uncertainties," IEEE Transactions on Industrial Electronics, vol. 63, no. 10, pp. 6429–6438, Oct. 2016.
- [57] Petter lunderstrom , sigurd Skogestad and Zi-Qin Wang,"Performance Weight Selection for H-Infinity and μ -Control Methods", Transaction of the Institute of Measurement and Control, pp.241-252, December 1-1991.
- [58] V. Kneppova, U.Kiffmeier and H.Unbehauen," Weight Function Selection in H_∞ -Optimal Control with Application To A Thyristor Driven DC Motor", American control conference, June 1995.
- [59] L.Sedghi and A.Fakherian,"Robust Voltage Regulation in Islanded Microgrids: A LMI Based Mixed H_2/H_∞ Control Approach", 24th Mediterranean Conference on Control and Automation (MED), June 21-24, 2016, Athens, Greece.
- [60] V. Grigore, J. Hatonen, J. Kyyra, and T. Suntio, "Dynamics of a buck converter with a constant power load," PESC 98 Record. 29th Annual IEEE Power Electronics Specialists Conference (Cat. No.98CH36196).,pp.1982-1986, July 2017.
- [61] Marian K. Kazimierczuk," Pulse-Width Modulated DC-DC Power Converters", second Edition, Wiley, October 2015.
- [62] Kemin Zhou, John C. Doyle and Keith Glover," Robust and optimal control", Prentice-Hall, Inc. Upper Saddle River, NJ, USA ©1996, ISBN:0-13-456567-3.
- [63] X. Zhang, X. Ruan, and Q. Zhong, "Improving the Stability of Cascaded DC/DC Converter Systems via Shaping the Input Impedance of the Load Converter With a Parallel or Series Virtual Impedance," IEEE Trans. Ind. Electron., vol. 62, no. 12, pp. 7499–7512, Dec. 2015.

693

694 **Appendix:**

695 **Definition2:** assuming $G(s)$ is a transfer function. The singular value of $G(s)$ is given by the
 696 square root of $G^*(s) \cdot G(s)$ eigenvalues, they expressed as:

$$\sigma(s) = \sqrt{\lambda(G^*(s) \cdot G(s))} \quad (44)$$

697 Denoting: $\underline{\sigma}(s)$ is the smallest singular value and $\bar{\sigma}(s)$ is the biggest singular value over all
 698 frequencies. Some singular value proprieties are given below:

$$\sigma(G(s)) = 0 \rightarrow G(s) = 0 \quad (45)$$

$$\forall \lambda \in \mathbb{C} \rightarrow \sigma(\lambda \cdot G(s)) = \lambda \cdot \sigma(G(s)) \quad (46)$$

$$\bar{\sigma}(A + B) \leq \bar{\sigma}(A) + \bar{\sigma}(B) \quad (47)$$

$$\bar{\sigma}(A \cdot B) \leq \bar{\sigma}(A) \cdot \bar{\sigma}(B) \quad (48)$$

$$\underline{\sigma}(A \cdot B) \leq \underline{\sigma}(A) \cdot \underline{\sigma}(B) \quad (49)$$

699 The H_∞ norm is defined as the biggest singular value.

$$\|G(s)\|_\infty = \bar{\sigma}(G(s)) \quad (50)$$

700 **Definition 3:** assume A, Q, and R be real (n x n) matrices. Q and R are symmetric. Then an
 701 algebraic Reccati equation is the following matrix equation:

$$A^* \cdot X + X \cdot A + X \cdot R \cdot X + Q = 0 \quad (51)$$

702 associated with (38) is a (2n x 2n) matrix:

$$H = \begin{bmatrix} A & R \\ -Q & A^* \end{bmatrix} \quad (52)$$

703 The matrix (53) is called a Hamiltonian matrix, which is used to obtain the solution to (52).
 704 The theorems are delivered in [56], give a way in terms of the invariant subspace of H for
 705 finding the solution to (52).

706 **Definition 4:** let $G(s)$ be a complex matrix partitioned as:

$$G(s) = \begin{bmatrix} G_{11}(s) & G_{12}(s) \\ G_{21}(s) & G_{22}(s) \end{bmatrix} \in \mathbb{C}^{(m_1+m_2)(q_1+q_2)} \quad (53)$$

707 and let $K(s)$ belongs to $\mathbb{C}^{q_2 \times m_2}$ be another complex matrix. Then, we can officially define a
 708 lower LFT as:

$$F_l(P, K) = G_{11}(s) + G_{12}(s) \cdot K \cdot (I - G_{22}(s) \cdot K)^{-1} \cdot G_{21}(s) \quad (54)$$

Theorem 1: the GD!!!OA is based on the solutions of two algebraic Reccati equations (see (56) and (57)). Taking into account the state space of the augmented system $P(s)$ described in (35), there are important assumptions to satisfy them, which are:

Assumption 1: (A, B_2) is stabilizable and (A, C_2) is detectable.

Assumption 2: $\text{Rank}(D_{11}) = n_w$ and $\text{Rank}(D_{12}) = n_u$.

Assumption 3: $\forall \Omega \in R \quad \text{rank} \begin{pmatrix} A - j \cdot \Omega \cdot I_n & B_2 \\ C_1 & D_{12} \end{pmatrix} = n + n_y$.

Assumption 4: $D_{12}^* \cdot [C_1 \quad D_{21}] = \begin{bmatrix} 0 \\ I_{n_u} \end{bmatrix}$

Assumption 6: $\begin{pmatrix} D_1 \\ D_{21} \end{pmatrix} \cdot D_{21}^* = \begin{pmatrix} 0 \\ I_{n_y} \end{pmatrix}$.

where: n_y , n_u and n_w are the lengths of y and u vectors and n is the order of the augmented system $P(s)$.

Theorem 2: the robust controller can be designed based on H_∞ norm if and only if the conditions below are satisfied. The matrices J_∞ and H_∞ are defined as follows:

$$H_\infty = \begin{bmatrix} A & \gamma^{-2} \cdot B_1 \cdot B_1^* - B_2 \cdot B_2^* \\ -C_1^* \cdot C_1 & -A^* \end{bmatrix} \quad (55)$$

$$J_\infty = \begin{bmatrix} A^* & \gamma^{-2} \cdot C_1^* \cdot C_1 - C_2^* \cdot C_2 \\ -B_1 \cdot B_1^* & -A \end{bmatrix} \quad (56)$$

Condition 1. J_∞ and H_∞ must not have the eigenvalues in the imagery axis.

Condition 2. X_∞ and Y_∞ are the solutions of the algebraic Reccati equations associated with (41) and (42); these solutions must be positive and different to zero.

Condition 3. $\lambda(X_\infty \cdot Y_\infty) > 0$.

Theorem 3: the designed robust controller-based H_∞ norm stabilizing the studied system must satisfy the condition:

$$\|F_l(P(s), K_\infty(s))\|_\infty \leq \gamma \quad (57)$$

the mathematical expression of the robust controller is given by:

$$K_\infty(s) = F_l(K_a(s), \Phi(s)) \quad (58)$$

where

$$[K_\infty(s)] = \left[\begin{array}{c|c|c} \underline{A_\infty} & \underline{Z_\infty \cdot Y_\infty \cdot C_2^*} & \underline{Z_\infty \cdot B_2} \\ -B_2^* \cdot X_\infty & 0 & I_{n_u} \\ -C_2 & I_{n_y} & 0 \end{array} \right] \quad (59)$$

$$\tilde{A}_\infty = A + \gamma^{-2} \cdot B_1 \cdot B_1^* \cdot X_\infty - B_2 \cdot B_2^* \cdot X_\infty - Z_\infty \cdot Y_\infty \cdot C_1^* \cdot C \quad (60)$$

$$Z_\infty = (I_n - \gamma^{-2} \cdot Y_\infty \cdot X_\infty)^{-1} \quad (61)$$

Highlights

- Constant power load and overall disturbances lead to lose the system performances.
- System modelling considers the uncertain parameters and whole disturbances.
- H_∞ controller enables mitigating the constant power load and disturbances effects.

Declaration of interests

☒ The authors declare that they have no known competing financial interests or personal relationships that could have appeared to influence the work reported in this paper.

☐ The authors declare the following financial interests/personal relationships, which may be considered as potential competing interests:

--